01 Nov 1968

Behavior of steel building connections subjected to inelastic strain reversals

E. P. Popov

R. B. Pinkney

Recommended Citation

STEEL RESEARCH for construction

BEHAVIOR OF STEEL BUILDING CONNECTIONS SUBJECTED TO INELASTIC STRAIN REVERSALS

E. P. Popov
R. B. Pinkney

BEHAVIOR OF STEEL BUILDING CONNECTIONS SUBJECTED TO INELASTIC STRAIN REVERSALS

by

E. P. POPOV

Faculty Investigator

and

R. B. PINKNEY

Research Assistant

DEPARTMENT OF CIVIL ENGINEERING
UNIVERSITY OF CALIFORNIA
BERKELEY, CALIFORNIA

PREFACE

This report is one of two prepared for American Iron and Steel Institute to summarize the results obtained from Research Project 120, sponsored by AISI. In this volume are presented an interpretation of the experimental results and suggestions for relating the results to actual design. In the companion volume, AISI Bulletin 14 entitled "Behavior of Steel Building Connections Subjected to Repeated Inelastic Strain Reversal—Experimental Data," are assembled the principal experimental results. Those interested in a detailed description of each experiment, including original and reduced data and photographs, should consult the latter report (available on request from AISI).

It is hoped that the results obtained and the conclusions reached during the course of this investigation will be of immediate usefulness to the designer of structural steel building frames in seismic regions.

ABSTRACT

Inelastic design of steel structures to withstand seismic forces requires a knowledge of the behavior of connections when subjected to cyclically reversed loading. This report contains a description of the design and testing of selected steel beam-to-column connection specimens. The motivations for the choice of connection types and overall geometry of the specimens are discussed, relating them to full-size prototypes used in actual building frames.

The characteristics of the test installation are described, including means of loading, type of lateral support provided, etc. The programs of cycling of all tests are presented in terms of the deflection of the tip of the cantilever beam. Typical hysteresis diagrams and failure photographs are also included. The outstanding features of the behavior of several specimens during testing are discussed and compared, and possible explanations given for particular aspects. Finally, the results of all of the tests are summarized, and an attempt made to draw comparisons and conclusions of somewhat broader applicability.

CONTENTS

LIST OF TABLES

LIST OF FIGURES

NOMENCLATURE

N number of inelastic cycles to failure

P concentrated load applied to free end of cantilever

P_p plastic load, computed from actual section and material properties

W energy dissipated during a single excursion

e energy ratio: $e = W/(\frac{1}{2}P_p \Delta_p)$ (denoted $\overline{W}$ in Report No. SESM 67-31—*Experimental Data*—AISI *Bulletin* 16)

r Ramberg-Osgood exponent

Δ deflection of free end of cantilever

Δ_p fictitious elastic deflection corresponding to plastic load P_p

Δ^1 residual deflection after one excursion

α Ramberg-Osgood parameter

β slope factor relating slope of unloading P-Δ curve to initial elastic slope

μ ductility ratio

π_d plasticity ratio, subscript denoting deflection measure (denoted $\overline{\Delta^1}$ in Report No. SESM 67-31—*Experimental Data*—AISI *Bulletin* 16)

σ_y yield strength (stress)

INTRODUCTION

Ever since the first use of rational procedures in the engineering design of steel structures, the elastic method of analysis has predominated. With the recognition of the remarkable ductility of low carbon steel, however, plastic methods of analysis have gradually gained favor. There are two principal reasons for this development. First, for statically applied loads, the predictions of the ultimate or limit capacities of members and frames are in excellent agreement with their actual behavior. Second, the resulting designs are usually lighter. Hence a greater economy of material is achieved as compared with equivalent designs based on elastic concepts. The status of the plastic method of analysis of steel structures has been summarized[1]* in the ASCE Manual of Engineering Practice No. 41, entitled "Commentary on Plastic Design in Steel." Plastic analysis is also discussed in a number of specialized[2,3,4] and general[5,6,7] textbooks.

For the most part, plastic analysis and design has in the past been directed toward the study of proportional, monotonically increasing loading: the loads are assumed to maintain a fixed ratio or proportion to one another and, once applied, continue to increase in magnitude until failure of a beam or frame occurs. This type of loading was found to be not entirely realistic for many applications, however, so study of variable, repeated loading ensued. In the classical paper[8] on this subject, P. S. Symonds and B. G. Neal described two possible situations which may obtain in a structure subjected to such loadings, and developed the concepts of shakedown analysis[1,4]. For arbitrarily varying and repeated loading, then, it is possible to determine the safe range of magnitudes between which the applied loads may vary. On the one hand, it is possible to determine applied loads of such a magnitude that the stresses they produce, superposed on the residual stresses, do not exceed the plastic capacity of a member. On the other hand, the loads can be

so limited that after several cycles, no additional inelastic deflection takes place. The first case is referred to as alternating plasticity; the second, as incremental collapse or deflection stability. While both of these criteria enlarge the scope of plastic analysis, they do not go far enough for some applications; both define a structure which ultimately responds elastically, after a few cycles of inelastic action.

None of the above approaches is sufficiently descriptive of some of the situations encountered in the structural design of steel buildings. In particular, the important case of the inelastic behavior of structural steel frames during an earthquake cannot be adequately treated. When a seismic disturbance occurs, the ground motion causes the building to vibrate, and both beams and columns become subjected to repeated and reversed loadings. In severe earthquakes, such loadings may induce repeated inelastic action in the structure. This has motivated study of steel members and connections subjected to repeated and reversed loading. Except for an earlier paper[9] by V. V. Bertero and E. P. Popov, no tests of this type appear to have been conducted in the United States. However, intensive research into the problem has been carried out in Japan. As results of this research may not be readily available to many American readers, a summary of the principal investigations has been prepared and is contained in the Appendix to this report. The broad scope of the Japanese work is to be noted: both steel members and assemblages have been investigated. The variety of member shapes, joint configurations and assemblages which have been studied can be readily seen from the sketches in the Appendix. In many of the tests, the type and sequence of loading was varied.

Since much of the inelastic action during an earthquake occurs at the joints of a structure, the present study was undertaken to investigate the behavior of beam-to-column connections subjected to repeated and reversed loading. A preliminary report[10] on this

---

*Refers to bibliography at the end of the report.

1

study was presented in the summer of 1965, followed by a progress report[11] in October, 1965, a paper[12] in September, 1966, and a presentation[13] at the National Meeting of the American Society of Civil Engineers in May, 1967. In this research project, twenty-four connection specimens were prepared and subjected to various loading sequences.

Because it is the current practice to design columns to remain elastic throughout an earthquake, the specimens were designed in such a way that the inelastic behavior would be confined to the beam. The same size beam was used throughout, but several different connection details were chosen, to reflect current American practice. The behavior of beams connected both to the column flange and to the column web was investigated. Two types of steel, ASTM A-36 and A-441, were used in different specimens. In addition to the behavior and the manner of failure of the beams and their connections to the columns, the hysteretic response of the beams under repeated and reversed loadings received particular attention in this investigation.

The hysteretic characteristics of metals, including steel, have been studied for a long time. Reliable information is available on the subject in numerous publications[14,15,16]. Usually, however, only the basic materials aspects of the problem are reported on, as derived from tests of polished specimens in a uniform stress field. In actual beam-to-column connections for buildings, several complications arise. Of practical necessity, the connections are made by welding or bolting. These details give rise to regions of high stress concentration. Moreover, structural steel members used in building construction consist of relatively thin components. When subjected to large compressive forces, flanges of rolled beams or fabricated plate girders tend to buckle. The overall hysteretic response obtained for a beam is strongly affected by these factors.

In the course of this research, numerous hysteresis diagrams or loops have been obtained for the applied load versus a characteristic deflection. These loops provide direct evidence of the energy dissipated in a struc-

tural steel member during a cycle of loading and unloading, for several types of realistic connections. The recorded results give an integrated response for the members and their connections, reflecting not only the material properties, but also the type of connection used and, at large strains, the effect of buckling of the flanges.

The type of information sought in this research program is essential in the dynamic analysis of buildings, as stiffnesses of members and damping characteristics of structural systems are directly related to the information provided by the hysteresis loops. Work on damped vibration analysis of building frames has been attempted by several investigators[17-21] and is currently an active field of research. It is hoped that the information presented in this report will aid in such analyses, resulting in better and safer design of high-rise structural steel building frames.

Detailed results of the experimental program may be found in the companion volume to this report, Reference 22.

SELECTION AND DESIGN OF SPECIMENS

The beam size selected for this series of experiments was 8 WF 20. The proportions of this section are such that the b/t ratio is similar to that of representative floor beams used in high-rise steel buildings. Although this member has a depth of only about one-third that of beams used in actual construction, it is sufficiently large to require no specialized fabrication procedures. The beam was attached as a cantilever to a short column stub, as shown in Fig. 1.

All column stubs were fabricated from 8 WF 48 sections. This resulted in a column stub of considerable relative rigidity and minimized the rotation of the cantilever at its support. It also achieved the desired behavior in that for all practical purposes, the stresses in the column stub remained elastic during an experiment.

The length of the cantilever was chosen to be approximately the scaled-down half-span length of a representative prototype. The application of a concentrated reversible load
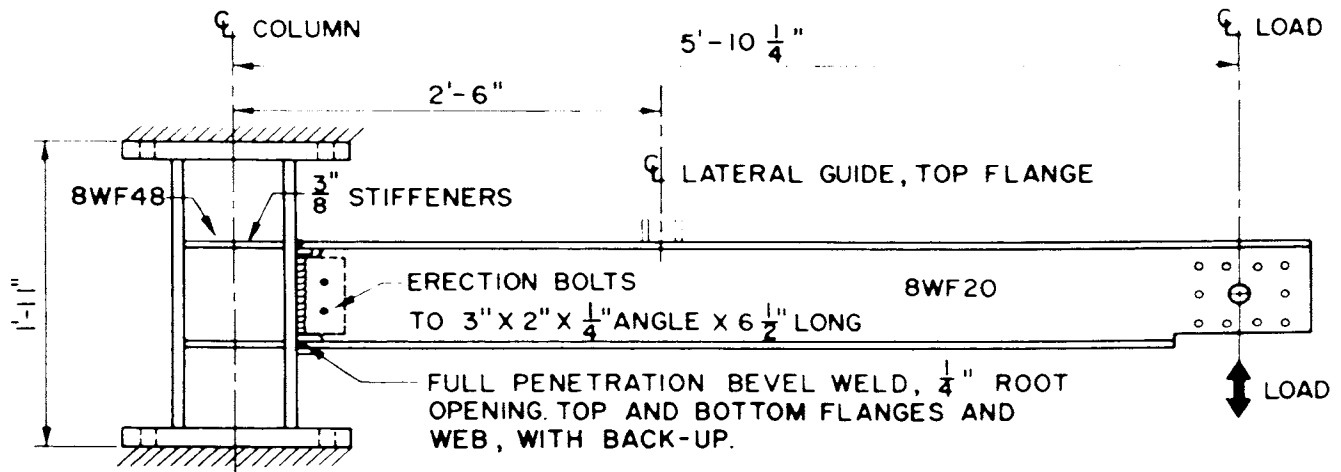
Fig. 1   Specimen type F1.

at the end of the cantilever was intended to simulate the distribution of bending moment produced in a typical beam by a lateral load on a structure. This distribution neglects the effect of gravity loading. as does the subsequent practice of applying equal and opposite cyclic forces to the specimen.

Five different basic connection types were investigated. In three of these, designated respectively as F1, F2 and F3, the beam was connected to the flange of the column. In the remaining two, designated W1 and W2, the beam was connected indirectly to the web of the column. All of the connection details were chosen on the basis of their practicability and their widespread use.

Connection Type F1

The simplest and perhaps most widely used flange connection is Type F1, shown in Fig. 1. The entire capacity of the member is developed by means of full-penetration single-bevel groove welds applied to both flanges and web. Since all welding is done in the field, an erection clip angle is provided for temporary bolting and as a back-up for the vertical web weld. This connection has been adopted in this report as the standard against which comparisons are made.

Connection Type F2

Another basic flange connection is Type F2, shown in Fig. 2. In this connection, moment transfer is effected by top and bottom flange plates. The rectangular bottom plate is shop-welded to the column by means

of a full-penetration singe-bevel groove weld. An erection clip angle functions exactly as for Type F1.

At erection time, the lower flange is fillet-welded to the bottom plate, the tapered top plate is butt-welded to the column and fillet-welded to the beam flange. The top plate is designed such that at a certain so-called "critical section," the flexural capacity of the plates matches that of the beam section. It is then customary to extend the welds beyond this design critical section.
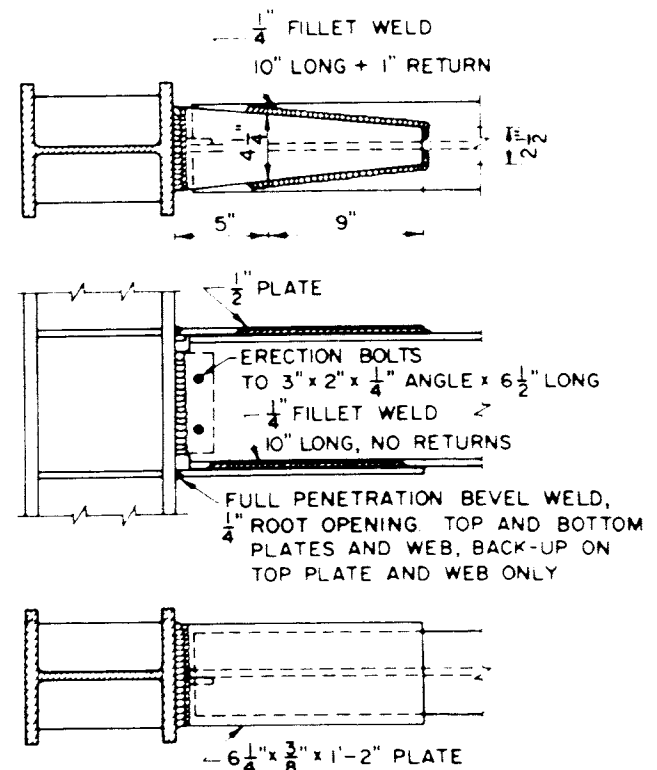

Fig. 2   Connection type F2.

3

Connection Type F3

The third flange connection, Type F3, shown in Fig. 3, makes use of high strength bolts for stress transfer. Top and bottom flange plates and web angle are shop-welded to the column, so that only bolting is necessary in the field. In this case, the web angle is used for shear transfer as well as erection convenience. Since vertical clearance between beam and plates is ordinarily provided for ease of erection, a thin, loose filler plate is included at the top flange.

Modified Connection Types

In lateral force design of a building, beam size is frequently dictated by drift limitation rather than strength. In this case, a connection is sometimes designed to develop only the calculated stresses, and not the full strength of the connecting beam. To examine the behavior of such a connection, two specimens of Type F2 were fabricated with arbitrarily thinner connecting plates. Designated as F2A and F2B, they had top and bottom plates 1/16 and 1/8 in. thinner, respectively, than the corresponding plates of Type F2. All other details remained unchanged.

The Type F3 specimens were designed such that the capacity of net section of the plates matched the capacity of the gross section of the beam, since there is evidence[2][3] that the latter may be fully developed in spite of the presence of holes. On the basis of the
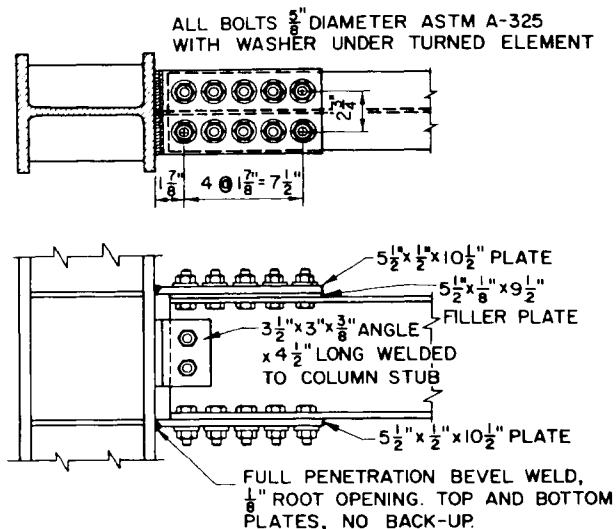

Fig. 3   Connection type F3.

net section of the beam, however, the connection was considerably over-designed. To compare the behavior of connections with the connecting plates designed by different criteria, therefore, two specimens of Type F3 were also fabricated with arbitrarily thinner flange plates. One of these, designated F3A, had connection plates nominally 1/16 in. thinner than those of F3. It was under-designed on the basis of gross section, and over-designed on the basis of net section, of the beam. The other, designated F3B, had plates nominally 1/8 in. thinner than had F3. This connection was considerably under-designed on the basis of gross section, but only slightly so on the basis of net section, of the beam.

TABLE I: Nominal properties of connection plates

Type	Top Plate Thickness	Bottom Plate Thickness	Min. Section Modulus*	Strength Factor**
F2	1/2 in.	3/8 in.	17.3 in.^{3}	1.02
F2A	7/16 in.	5/16 in.	15.1 in.^{3}	0.89
F2B	3/8 in.	1/4 in.	12.8 in.^{3}	0.75
F3	1/2 in.	1/2 in.	17.1 in.^{3}	1.01, 1.31†
F3A	7/16 in.	7/16 in.	14.9 in.^{3}	0.87, 1.14†
F3B	3/8 in.	3/8 in.	12.8 in.^{3}	0.75, 0.97†

*At nominal critical section for F2's; at net section for F3's.
**Based on gross section of beam except as indicated.
†Based on net section of beam.

4

The interrelationships among the basic connections F2 and F3 and their modifications, F3A, F2B, F3A, and F3B, are summarized in Table 1. Note that these are nominal properties, based on specified dimensions.

Connection Type W1

The first of the web connections, Type W1, is widely used because of its simplicity. It is shown in Fig. 4. Flush stiffener plates, welded to both flanges and web of column, provide for a direct butt-welded connection to the beam flanges. The web plate provides for temporary erection bolting and transfers shear in the completed connection through a fillet weld to the beam web.

Connection Type W2

Instead of the flush stiffener plates used in Type W1, tapered or shaped plates are sometimes used, with the idea that a gradual change in the cross section of the beam flange should reduce the effects of stress concentration. Two specimens of this type were fabricated and designated W2. Specimen W2A had a tapered plate at the top flange and a shaped plate at the bottom, as shown in Fig. 5. Specimen W2B had exactly the reverse. It was thought that in this manner, a single specimen would provide information not only on the behavior of a web-connected beam, but would also point to any possible difference in performance between the two types of plate.

Fabrication of Specimens

Throughout fabrication of the specimens, an attempt was made to simulate the physical orientation and welding sequences found in actual construction. Weld back-ups were used only for field welds, and all welds which would be vertical were executed in that position. Professional inspection services were procured for many specimens.

Twenty-four specimens* were fabricated for the experimental program described in this report. The five basic connection types,

*One additional specimen was tested for the purpose of making a motion picture. As instrumentation was not complete for this test, the results are not reported herein. Its performance was typical of Type F1.
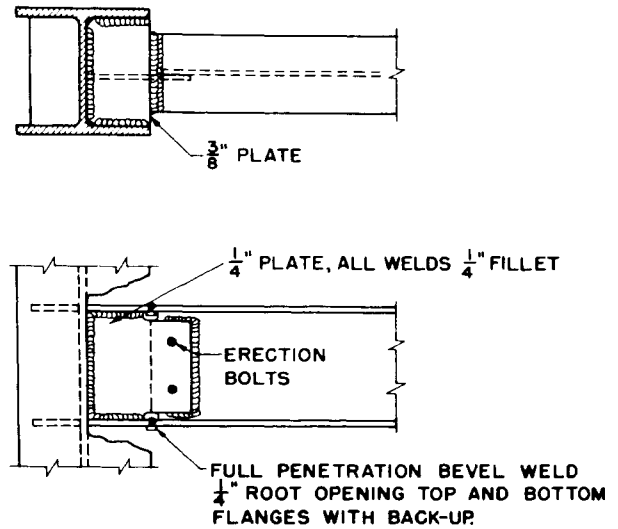

Fig. 4   Connection type W1.

together with the modified details for Types F2 and F3, constitute a total of nine different connections. Specimens of all these, with some duplicates, were made of ASTM A-36 steel. In addition, two each of Types F1 and F2 were made of higher strength ASTM A-441 steel. The latter are identified in the sequel by the letters HS, as F1HS and F2HS, respectively. The dimensions and details for these specimens were the same as for those of A-36 steel.
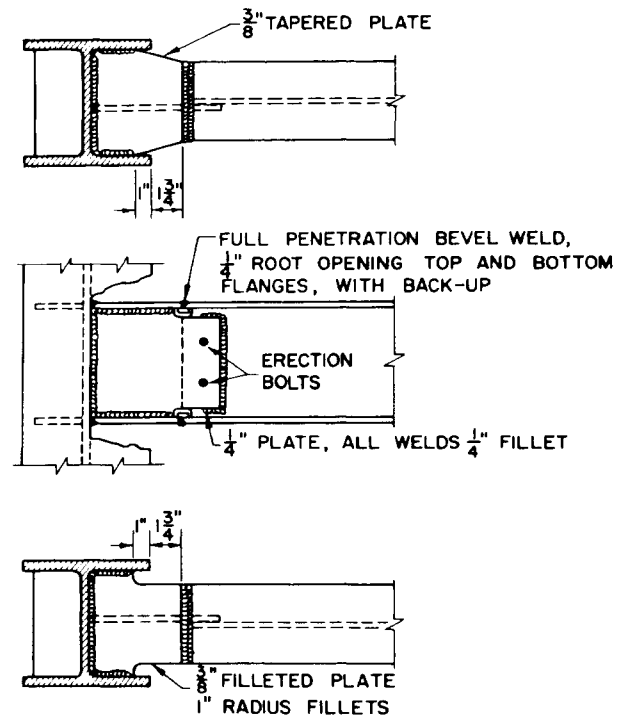

Fig. 5   Connection type W2A.

5

EXPERIMENTAL INSTALLATION

The principal features of the test fixture are shown schematically in Fig. 6. Provision was made to securely bolt the column stub to the frame, projecting the cantilever beam horizontally. Load was applied by means of a double-acting hydraulic cylinder. The actual installation was somewhat more elaborate, as can be seen from Fig. 7.

Lateral Guides

With the end of the cantilever corresponding to the midspan of a prototype beam, it was assumed that it would represent a point of inflection in a laterally loaded structure. Since in the prototype this point would therefore not tend to buckle sideways, a guide preventing both lateral and torsional displacement was provided at the end of the specimen. Further, since the top flange of a beam in a building is typically supported laterally by the floor system, a guide preventing lateral displacement of the top flange, but permitting twisting, was provided at the middle of the cantilever. The details of the two guides are shown in Fig. 8. To minimize friction, the guide races were heavily greased.

Load-Deflection Measurement

In the early experiments, the deflection of the cantilever tip (point of load) was measured intermittently by means of dial gages. It was soon found to be more advantageous to measure this deflection continuously using a multi-turn electrically linear potentiometer. The output from this instrument was connected to the horizontal input of an XY recorder. The vertical input of the recorder was taken from a load transducer inserted in series mechanically between the tip of the beam and the hydraulic cylinder. The transducer comprised a hollow aluminum cylinder with electrical strain gages as the sensitive elements, wired to provide two independent outputs. In all experiments, one of these outputs was monitored with an SR-4 strain indicator. The mechanically recorded output provided graphical hysteresis loops for applied load versus tip deflection.

Strain Measurements

In many cases, single-element electric strain gages were applied in the center of either the top or the bottom flange, or both, at an arbitrary distance from the face of the
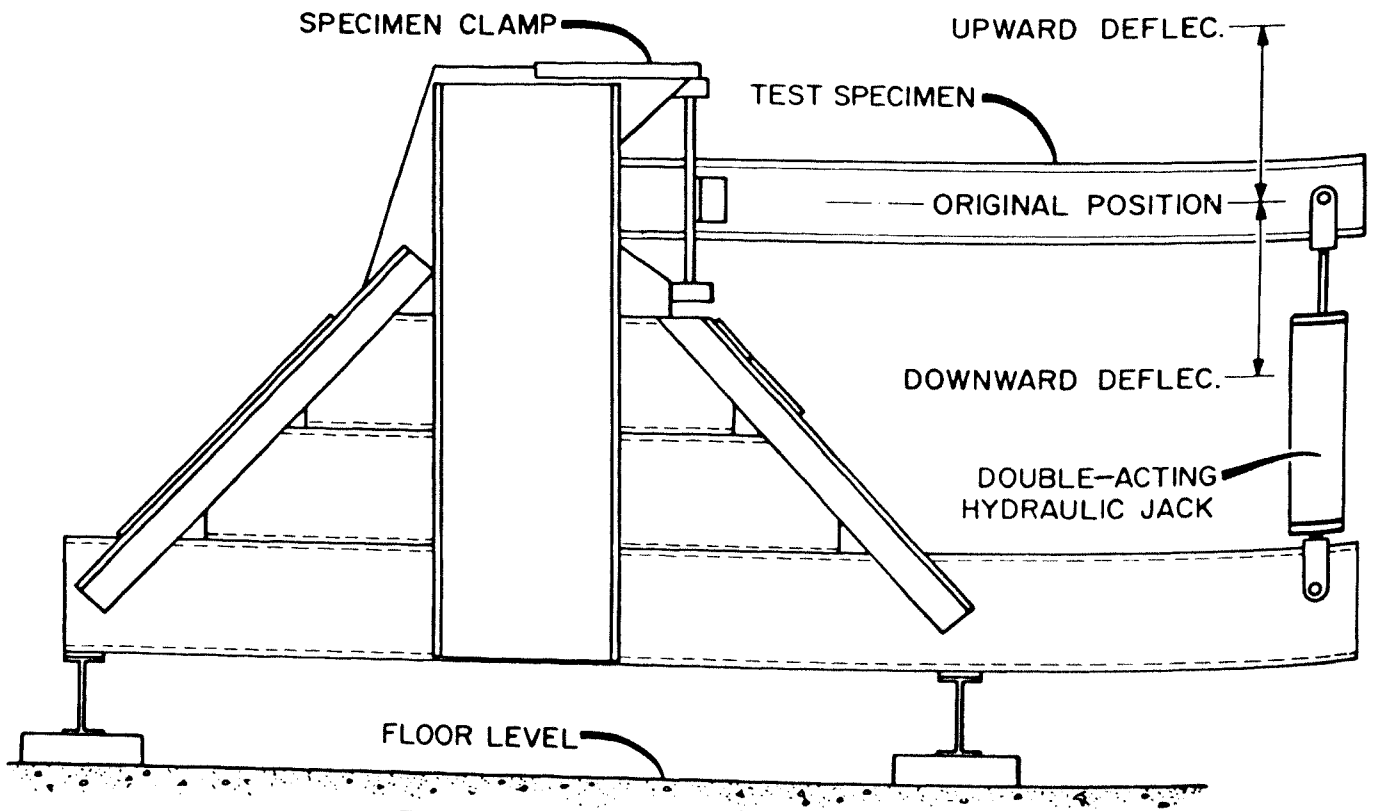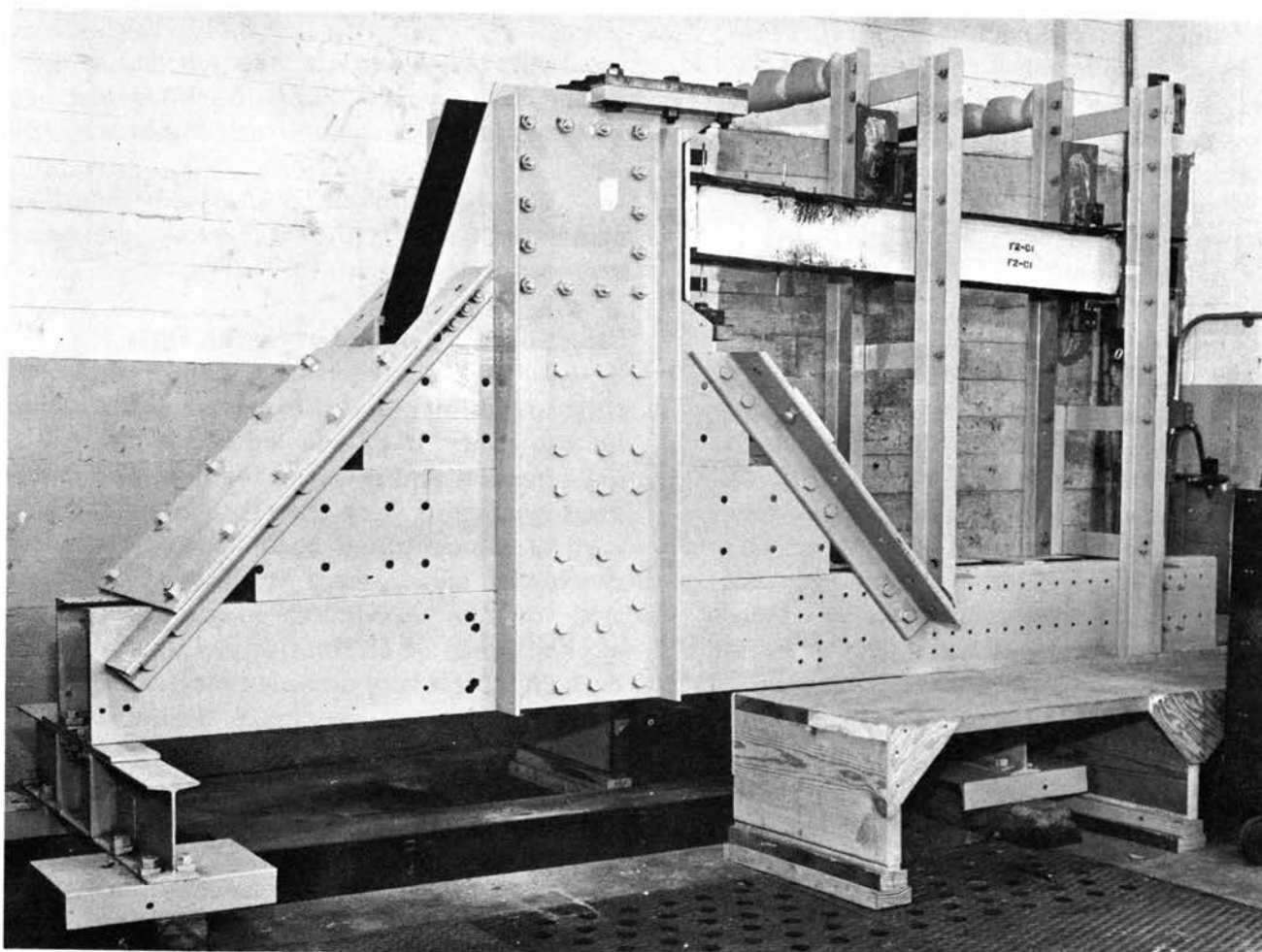

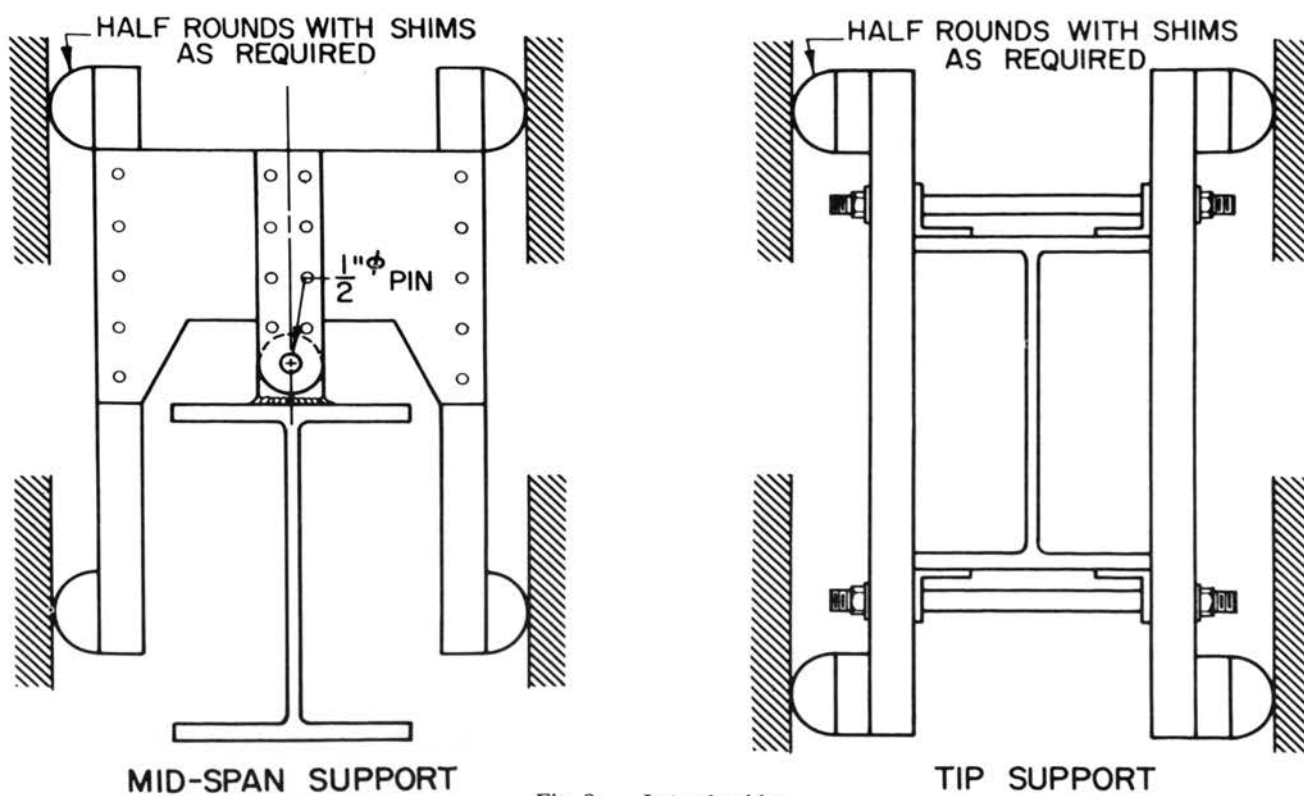Fig. 6   Schematic of test fixture.

Fig. 7   Test fixture with specimen.

HALF ROUNDS WITH SHIMS AS REQUIRED

$\frac{1}{2}"\phi$ PIN

MID-SPAN SUPPORT

HALF ROUNDS WITH SHIMS AS REQUIRED

TIP SUPPORT

Fig. 8   Lateral guides.

7

column stub. By connecting one of these gages to the horizontal input of an XY recorder, and the load to the vertical input, it was possible to trace graphical load-strain hysteresis loops. With suitable assumptions, these diagrams were used to determine moment-curvature relationships.

Numerous additional electrical strain gages were applied to many of the beams for specific purposes. In several experiments, gages were applied in pairs directly opposite each other on the inside and outside faces of a flange. The difference in readings from such gages is a sensitive indicator of buckling. In some experiments, several parallel gages were applied to the flanges to investigate the distribution of longitudinal strain. In still other experiments, gages and/or rosettes were attached to the web of the beam, and in a few cases, to the column stub.

EXPERIMENTAL PROCEDURE AND OBSERVATIONS

Static Test F1-S

Since most of the readily available experimental research on members and connections deals with a single application of a monotonically increasing load, such an experiment was performed for comparison on one of the Type F1 specimens. The load-deflection diagram for this experiment is shown in Fig. 9. Strictly speaking, this experiment was not truly monotonic with regard to the load application. During the experiment, the load was removed three times and reapplied. The reloading path was essentially the same as the unloading path. This is a well-known phenomenon and requires no further comment.

To obtain an idea of the strains developed in the specimens during the experiment, the output from an electric strain gage located at 1.50 inches from the column face at the center of the top flange was monitored. At about 0.2% strain, as measured by this gage, considerable yielding of the flanges and the web had occurred, as evidenced by peeling and cracking of the whitewash applied to the specimen. Strain hardening commenced at

about 1.5% strain, causing an increase of load until the test maximum was reached at 4.5% strain. Compression flange buckling was first observed when the monitored strain was near 1%.

The behavior of the specimen in this static test was typical of many prevously reported in the literature.

Selection and Control of Cyclic Tests

As stated earlier, the main purpose of these experiments was to obtain information on the behavior of selected connections during repeated and reversed loading. The cantilever specimens were therefore subjected to a vertical concentrated load applied cyclically downward and upward at the tip. The selection of the maximum magnitude of the applied load, or alternatively, the applied tip deflection, is a very complex matter. Whether, for example, the specimen should be subjected to large loads which cause fracture after but a few cycles; or to loads of moderate magnitude, associated with moderate deflections, which require a relatively large number of cycles to cause fracture; or to some arbitrary multiple of the deflections expected at working load, is a question which cannot be resolved in a simple fashion. There is interest in the manner of failure due to exceptionally high load, as may well prevail in an isolated joint of a building during an earthquake. There is interest in the longevity of a connection under substantial overloads. And for purposes of dynamic analysis of the overall structural behavior of a frame, there is interest in the amount of damping that can be relied upon immediately after the elastic range is exceeded.

In an attempt to answer at least partially the above and related questions, a variety of cyclic loading programs was devised. In most of the tests, the program of loading was such that a sequence of increasing strain or deflection amplitudes was applied, with an arbitrary number of cycles at each amplitude. However, as such regular increments in the control parameters are not necessarily characteristic of what may occur in a real structure, other cycling programs were also used. In some
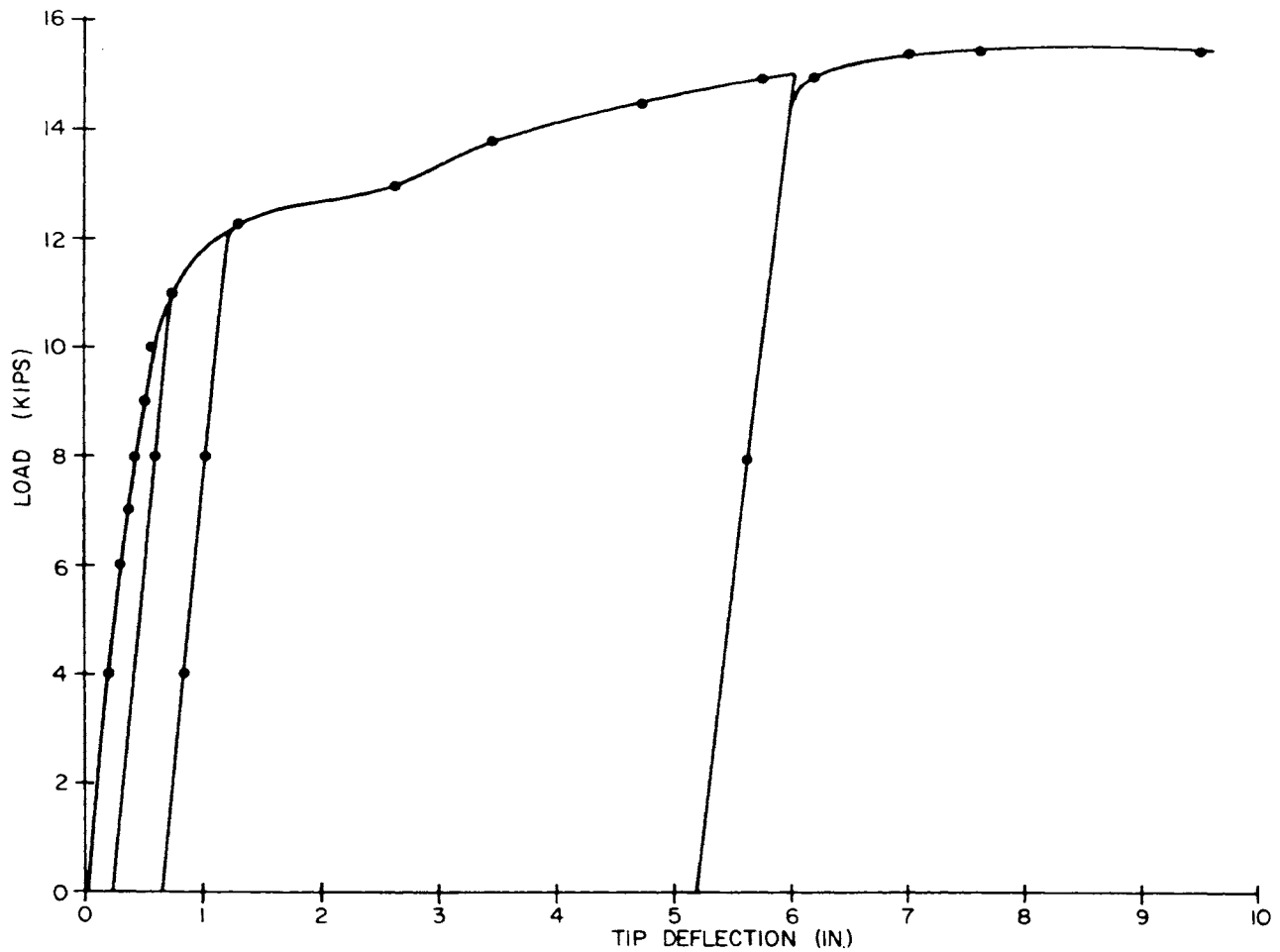
Fig. 9   Load vs. deflection—F1-S.

TABLE II: Identification of specimens and tests

Type of Connection	F1	direct butt-welded (flange-connected)
	F2	welded connecting plates (flange-connected)
	F3	bolted connecting plates (flange-connected)
	W1	flush connecting plates (web-connected)
	W2	tapered and filleted connecting plates (web-connected)

Type of Cycling	C1	five cycles each at nominal ±½% control strain increments
	C2	constant nominal ± 1½% control strain
	C3	100 cycles at constant nominal ± ½% control strain followed by constant ± 1½% nominal control strain
	C4	constant nominal ± 1% control strain
	C5	constant ± ½% nominal control strain
	C6	two cycles each at ± ¼% nominal control strain increments
	C7	fifteen cycles each at ± ½% nominal tip-deflection increments starting from ± 1 in.
	C8	same as C7
	C9	same as C7, except preceded by two cycles at ± 2 in. nominal tip deflection
	C10	same as C7, except preceded by five cycles at ± 2 in. nominal tip deflection
	C11	same as C7, except preceded by five cycles at ± 2½ in. nominal tip deflection

9

cases, a constant amplitude as applied throughout the test. In others, very large displacements were applied initially, followed by moderate, stepwise increasing amplitudes. Table II summarizes the nomenclature used to identify the specimens.

Each test began with the application of three complete cycles at a maximum nominal stress of 24 ksi. These cycles produced essentially elastic response, and served to check out the instrumentation.

The schematic diagrams for all of the cyclic tests, exclusive of the initial elastic cycles, are shown in Fig. 10. Each diagram clearly displays the maximum amplitudes of the tip-deflection and the number of inelastic excursions to failure. Note that the number of excursions into the plastic range is twice the number of cycles, N.

From Fig. 10 it can be seen that the desired tip-deflection was controlled more accurately in some tests than in others, assuming that it should have been constant for a given number of cycles. In fact, the earlier tests in the series, specifically C1 through C6, were controlled on the basis of strain, as measured on the beam flange at an arbitrary distance from the face of the column. In most of these, deterioration of the strain gage eventually required that cycling be controlled on the basis of tip-deflection. Although to some extent unsatisfactory, this technique provided a correlation between strain and deflection which was useful in planning subsequent tests. Beginning with the C7 program, tip-deflection control was used exclusively.

Typical Hysteresis Curves

Load-deflection data were acquired for every experiment with cyclically applied load. Representative hysteresis loops are shown in Figs. 11 through 14.

Hysteresis loops showed remarkable reproducibility during consecutive cycles of loading. As the areas enclosed by these loops correspond to the capacity of a member and its connection to absorb and dissipate energy, this indicates high dependability. The fatigue or work softening, which could sometimes be detected after a large number of cycles, was small and did not appear to be of much consequence.

The load-deflection hysteresis curves, in general, resemble the well-known ones for the material itself [15]. It is noteworthy, however, that the hysteresis loops in Fig. 11 remained stable even after severe buckling of the flanges had occurred. Such buckles were observed to appear and disappear cyclically, depending upon the sense of the applied load. Thus the beam and its connection were found to retain their load-carrying capacity even in the presence of pronounced buckling.

The hysteresis loops for bolted connections are unique. Slippage at the faying surfaces was responsible for the characteristic shape shown in Fig. 13. Three successive stages of structural action are discernible, static frictional resistance, active slip and bearing on the bolts. The holes for specimens F3-C1 and F3-C5 were punched the customary 1/16 in. oversize. The holes for specimens F3A-C7 and F3B-C7, on the other hand, were drilled 41/64 in. or 1/64 in. over the nominal bolt size of 5/8 in. As might be expected, the hysteresis loops for the latter two specimens exhibited a much smaller range of active slip, so that they approached the typical shape obtained for the other specimen types.

An example of hysteresis loops obtained for load versus strain measured at a selected location is shown in Fig. 15. In the absence of buckling, these curves may be interpreted as moment-curvature relationships. It is then possible to compute the load-deflection hysteresis loops, using the area-moment method [12]. During the time of this investigation, unfortunately, facilities were not available for determining cyclic stress-strain relationships from coupon specimens.

General Behavior and Failure of Connections

It is well known that members and connections can be subjected to an extremely large number of load reversals without distress, provided the elastic limit of the material is not exceeded. It appears that even if the elastic limit is exceeded slightly, the
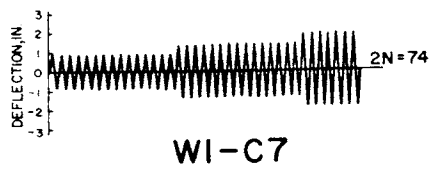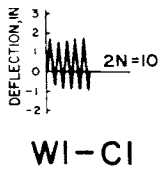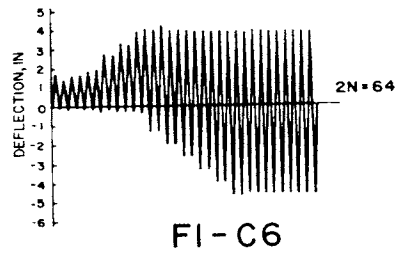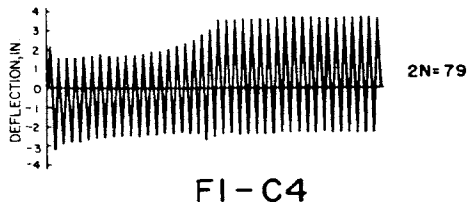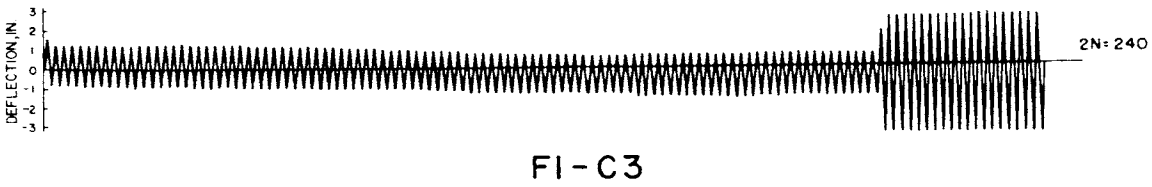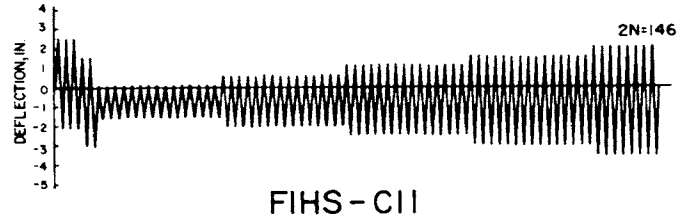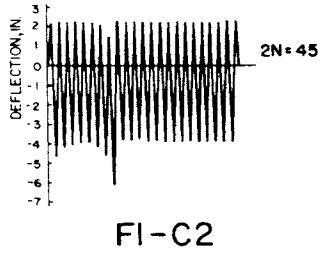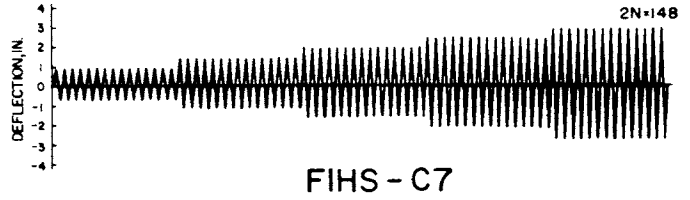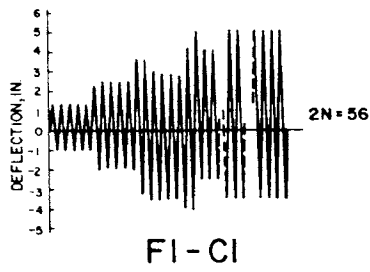
Fig. 10   Programs of cycling.
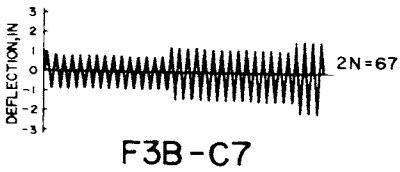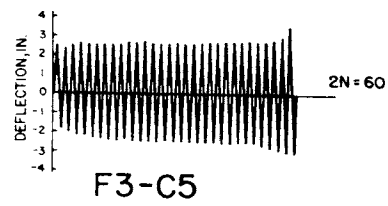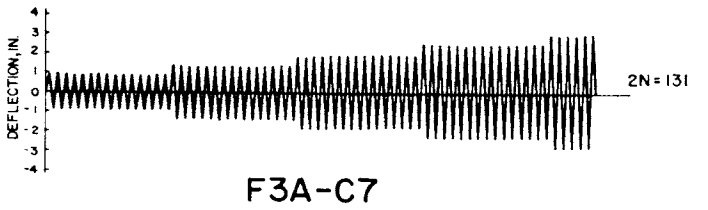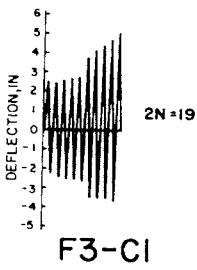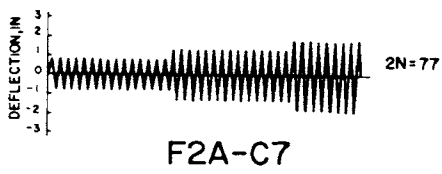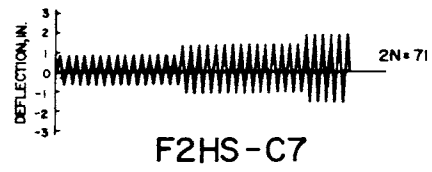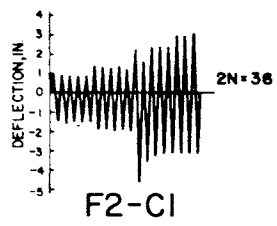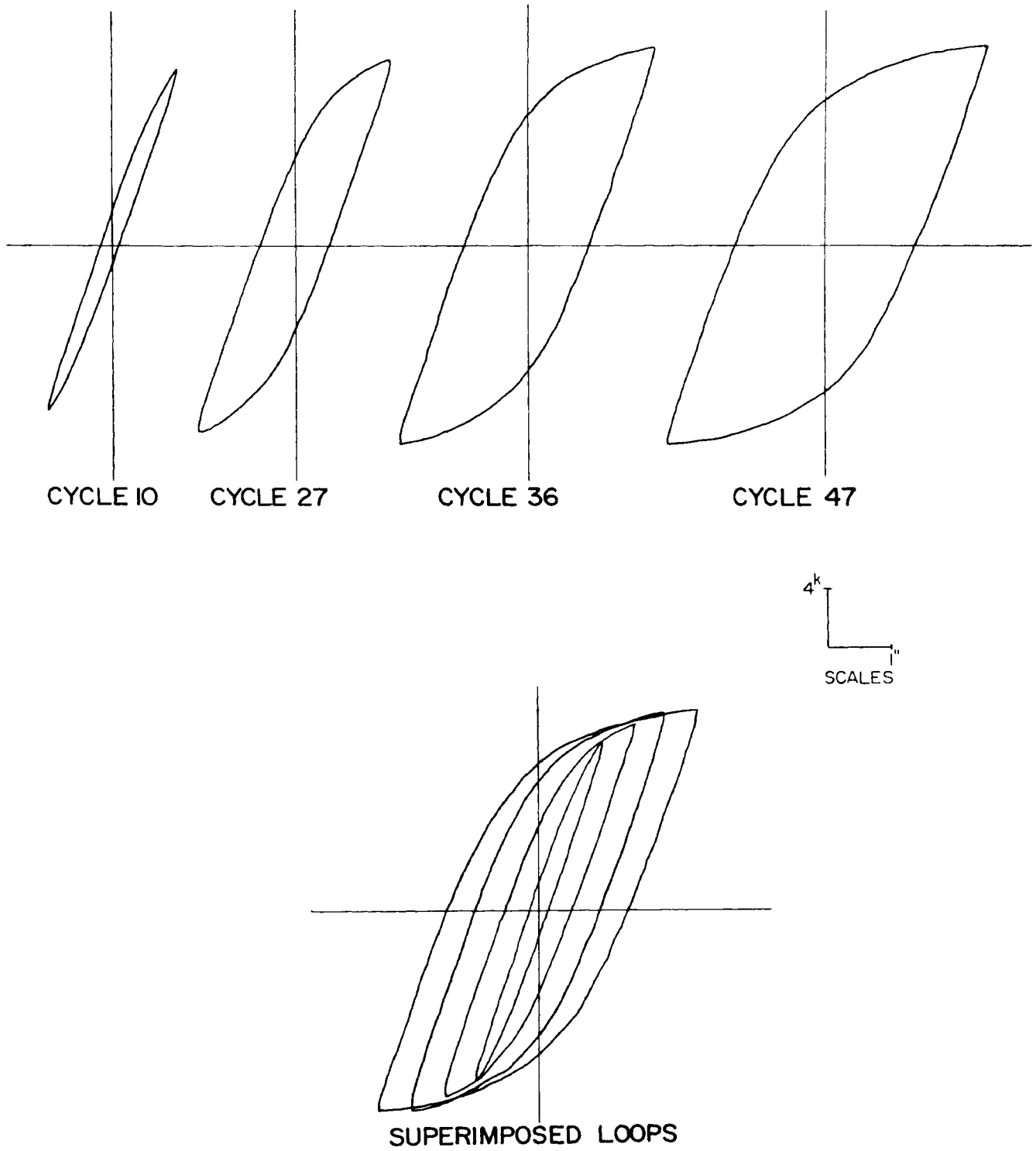
11

Fig. 10   (Continued)

CYCLE 10   CYCLE 27   CYCLE 36   CYCLE 47

SCALES

SUPERIMPOSED LOOPS

Fig. 11   Experimental load-deflection hysteresis loops for specimen F1HS-C7.

CYCLE 14   CYCLE 19   CYCLE 31

SCALES
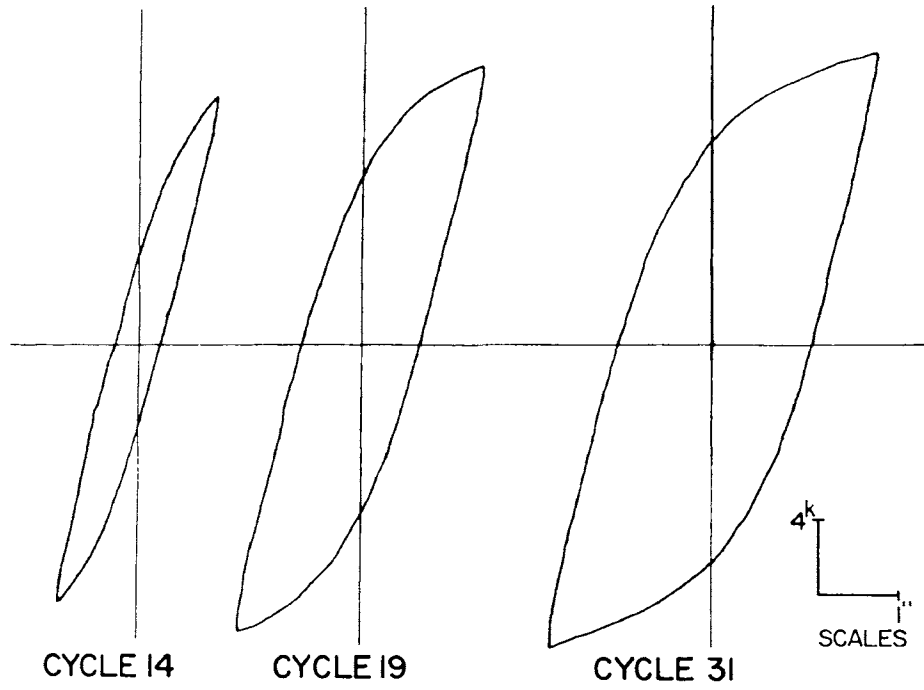
Fig. 12   Experimental load-deflection hysteresis loops for specimen F2A-C7.

CYCLES 1-3   CYCLES 4-6

SCALES
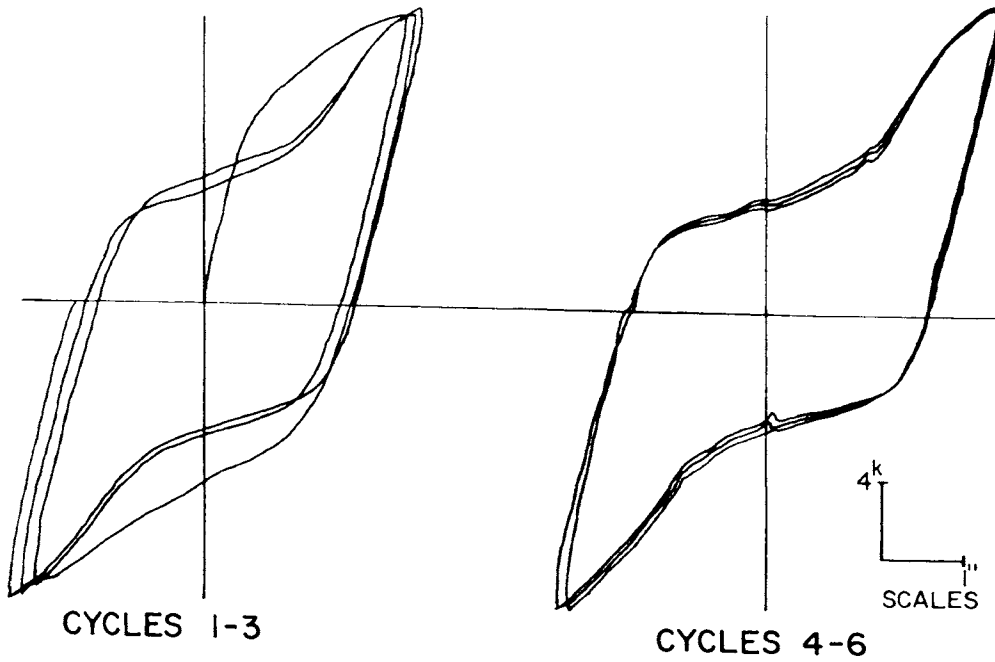
Fig. 13   Experimental load-deflection hysteresis loops for specimen F3-C5.

14

SCALES

4ᵏ
1"

CYCLES 1-5　　　　CYCLE 16　CYCLE 22　　　CYCLE 35

Fig. 14　Experimental load-deflection hysteresis loops for specimen W1-C9.

4ᵏ
1%

SCALES

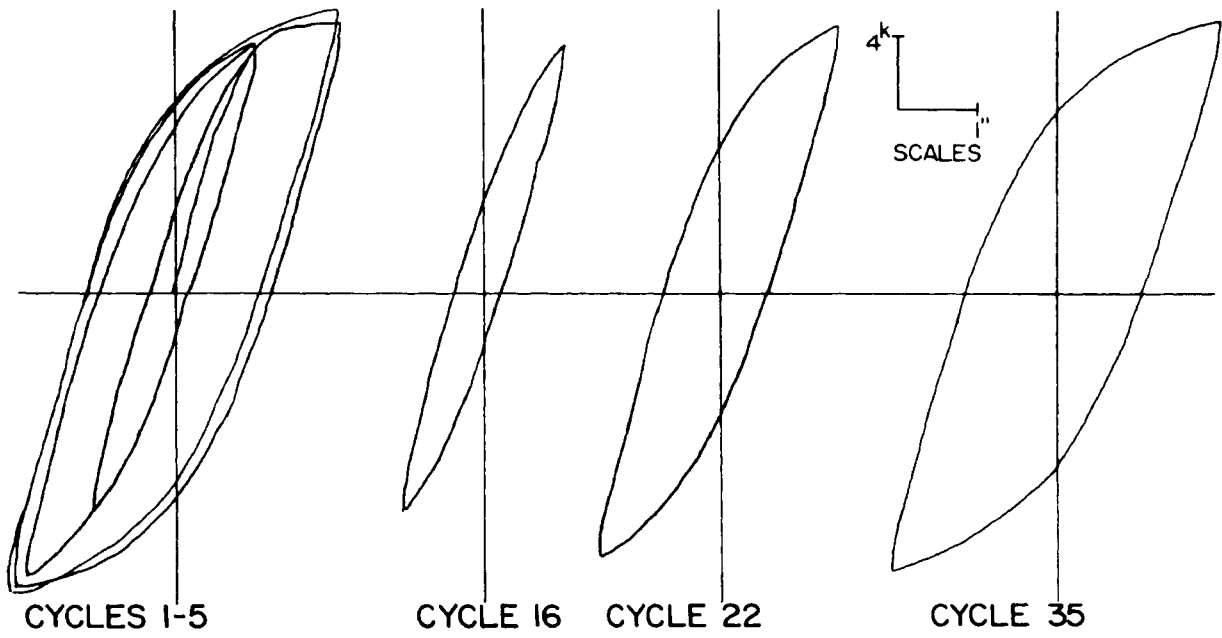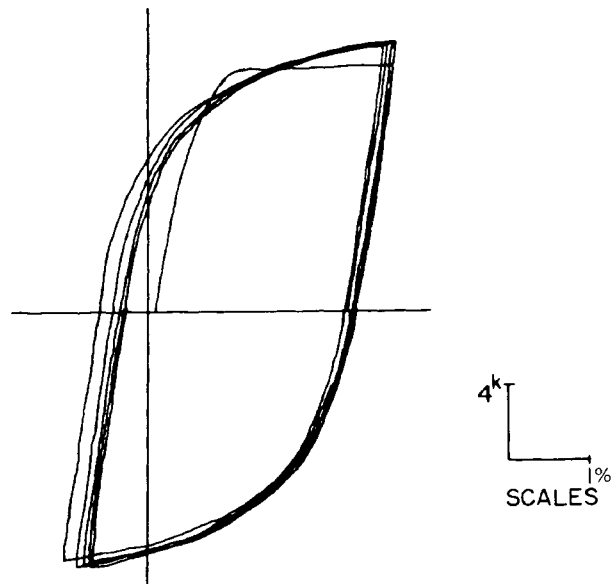Fig. 15　Experimental load-strain hysteresis loops for specimen F1-C1.

15

number of strain reversals before failure can still be very large. For example, specimen F1-C3 was subjected to one hundred cycles with a tip-deflection of about 2.6 times its maximum elastic deflection. At the end of this sequence, no significant deterioration was noted, either in the hysteresis loops or visually in the specimen itself. An additional twenty cycles of much greater severity were required to fracture the specimen.

Unlike the experiment on specimen F1-C3, most of the tests were designed to produce failures with a smaller number of cycles. This was accomplished by increasing the cycling amplitude at predetermined increments in the number of cycles. With this in mind, several observations will now be made concerning the specimen failures.

A specimen was deemed to have failed only when an increase in deflection was accompanied by a decrease in load, within the current cycling amplitude. There was some variation in the mode of failure, as can be seen in Figs. 16 through 19. Fracture was frequently in or near the welds, with several failures occurring in the butt-welds of the flanges to the column face in the case of Type F1. Where there were welded connection plates, as in Types F2, W1 and W2, cracks usually initiated at the ends of the welds and propagated into the connecting plates. In severely strained connections, cracks would often be initiated at several locations and would then merge to precipitate complete fracture.

In some specimens, cracks were initiated or aggravated by the tack-welds used to attach supplementary rotation instrumentation[22]. Sharp-cornered web copes were a recurring source for initiation of web cracks. A few specimens failed due to complete fracture of a flange at a buckled cross section. In general, crack propagation was slow.

The behavior of the bolted connections was quite different from that of the welded ones. As noted previously, slippage between the plates and flanges was a characteristic phenomenon, and was often accompanied by loud bangs during testing. In connections with heavy connection plates, such as F3-C1 and F3-C5, failure occurred in the beam flanges at the outermost bolt line. In the case of thinner plates, failure occurred through them at the bolt line nearest the column.

Specimens W1-C1 and W1-C4 failed prematurely due to poor workmanship during fabrication. Contrary to design specifications, only about one-half of the flange thickness was beveled to receive the weld. Moreover, the beams were jammed tight against the connecting plates prior to welding, eliminating any root opening. The result was that the welds penetrated only one-half the flange thickness, rather than the entire thickness, as specified. In subsequent ultrasonic inspection, the indications produced by the unwelded contact surface were mistakenly interpreted as being due to the back-up bars. The possibility of such an inspection error appears less likely for thicker material. Nevertheless, shop inspection prior to welding, not carried out in the fabrication of these two specimens, seems essential. The other web-connected specimens performed satisfactorily. The propensity for crack initiation in this type of connection appears, however, to be greater than in the flange-connected type.

Table III contains a brief description of the failure of each specimen.

DISCUSSION OF RESULTS

The quantitative treatment of fatigue phenomena has traditionally been probabilistic in nature, due to the inherent impossibility of exactly reproducing material and geometric properties, and experimental technique, in two or more specimens. Such treatment requires, of course, a statistically valid number of experiments, with as nearly identical as possible input parameters. Thus, although the present problem can be characterized in part as one of low-cycle fatigue, the number and variety of specimens and the lack of uniformity of experiments preclude the use of a statistical approach. Fatigue theory therefore cannot be used, and rational analysis directed toward the prediction of such fatigue characteristics as expected life is impossible.
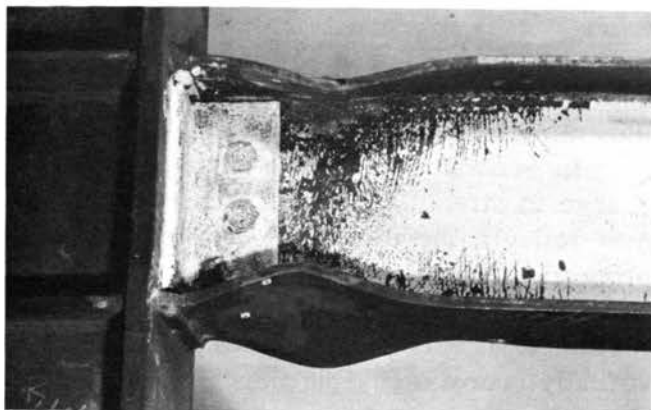
Fig. 16   Specimen F1HS-C11 at failure.

Fig. 17   Specimen F1-C1 at failure.

TABLE III: Mode of failure of specimens tested

| Specimen	Cycles to Failure	Description of Failure
F1-C1	28	Flange buckling; crack at buckle, bottom flange.
F1-C2	22½	Flange buckling; crack near bottom flange weld.
F1-C3	120	Flange buckling; crack at top flange weld.
F1-C4	39½	Flange buckling; crack at stud at bottom flange buckle.
F1-C6	32	Flange buckling; crack at top flange buckle.
F2-C1	18	Crack in top plate at end of weld.
F2-C4	44	Transverse crack in top plate at end of weld; longitudinal crack in top plate weld.
F2A-C7	38½	Plates buckled near column; crack at bottom plate buckle.
F2B-C8	32½	Bottom plate buckled near column; cracked at buckle and at weld.
F3-C1	9½	Slight buckling of flanges; crack in top flange at outermost bolt line.
F3-C5	30	Crack in top flange at outermost bolt line.
F3A-C7	65½	First crack in bottom flange, outermost bolt line; second crack in top plate at innermost bolt line; actually simultaneous failure.
F3B-C7	33½	Crack in bottom plate at innermost bolt line.
W1-C1	5	Crack at top flange weld; defective welding.
W1-C4	½	Crack at bottom flange weld; defective welding.
W1-C7	37	Crack from end of top flange weld into plate.
W1-C9	51½	Crack from end of bottom flange weld into plate.
W2A-C7	46½	Buckling of bottom plate; crack initiated at cutting torch gouge in bottom plate.
W2B-C10	30	Crack at weld in top plate.
F1HS-C7	74	Flange buckling; crack at top flange weld.
F1HS-C11	73	Flange buckling; crack near top flange weld.
F2HS-C7	35½	Slight buckling of flanges; complete longitudinal crack of one top plate fillet weld.
F2HS-C9	54½	Buckling of top flange and bottom plate; crack at bottom plate-to-column weld.

17
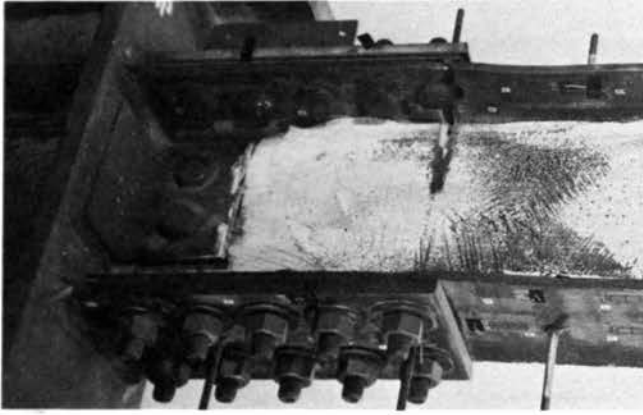
Fig. 18   Specimen F3-C1 at failure.

The following discussion, then, will be largely qualitative, except insofar as actual experimental data are presented.

Design Properties

Of primary concern to the designer are the strength and stiffness of a joint. Accordingly, the parameters which have been chosen to describe the design properties of a test specimen are the plastic load and the elastic stiffness, as computed from the actual geometry and material properties of the particular specimen. These parameters are represented
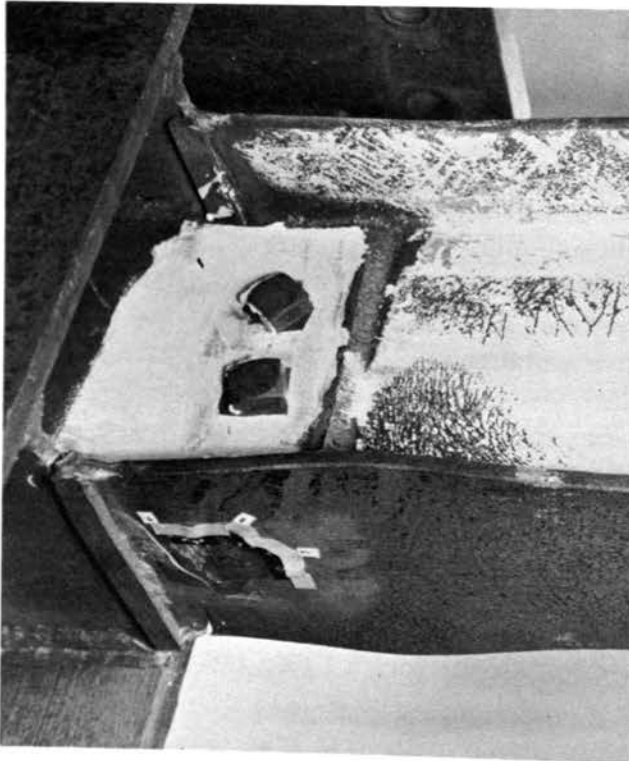

Fig. 19   Specimen W1-C9 at failure.

schematically in Fig. 20. Parameters for all of the actual specimens, relative to the as-detailed properties of specimen type F1, are illustrated in Fig. 21.

In general, for a given specimen type, a change in strength without a change in stiffness reflects the effect of different material properties. Simultaneous change of strength and stiffness reflects the effect of different geometry. This is because Young's modulus is virtually constant regardless of the yield strength of steel. Comparison of Type F1 with F1HS and Type F2 with F2HS clearly demonstrates this. It may be noted that while Types F2 and F3 both have higher stiffnesses than Type F1, the strength of Type F3 is lower, due to the reduced net section. Type W1 is comparable to Type F1, while Type W2 displays relatively lower stiffnesses as a result of the slightly increased free length of the beam. An attempt will be made later to assess the influence of the strength-stiffness relationships on the performance of the specimens.

Hysteresis Diagrams

The load-deflection hysteresis diagrams for a specimen contain considerable information about its performance. In addition to providing a continuous record of the relationship between load and deflection, the diagrams make it possible to determine the energy input to the specimen through integration of the work done by the external load.

Except for diagrams that display evidence of slippage, as do those for the Type F3 specimens, an analytical expression is available for the description of the typical non-linear load-deflection relationship. Conceived
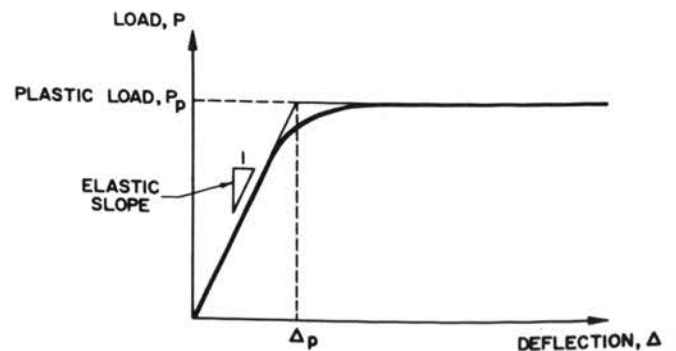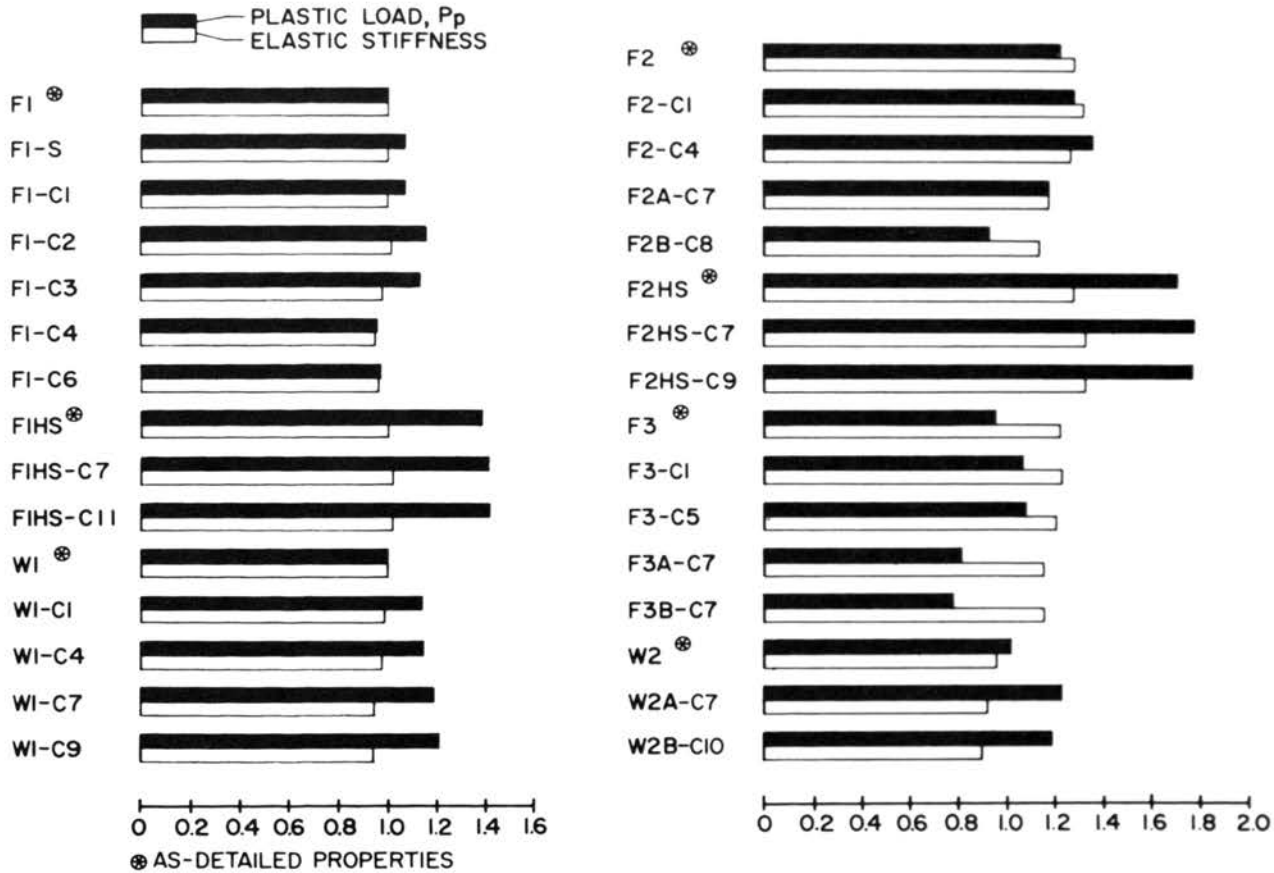

Fig. 20   Design parameters.

18

PLASTIC LOAD, P_p
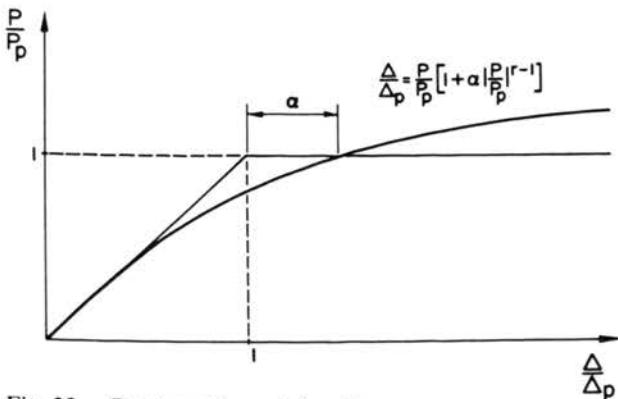ELASTIC STIFFNESS

F1 ⊛
F1-S
F1-C1
F1-C2
F1-C3
F1-C4
F1-C6
F1HS ⊛
F1HS-C7
F1HS-C11
W1 ⊛
W1-C1
W1-C4
W1-C7
W1-C9

F2 ⊛
F2-C1
F2-C4
F2A-C7
F2B-C8
F2HS ⊛
F2HS-C7
F2HS-C9
F3 ⊛
F3-C1
F3-C5
F3A-C7
F3B-C7
W2 ⊛
W2A-C7
W2B-C10

0   0.2 0.4 0.6 0.8 1.0 1.2 1.4 1.6

⊛ AS-DETAILED PROPERTIES

0   0.2 0.4 0.6 0.8 1.0 1.2 1.4 1.6 1.8 2.0

Fig. 21   Properties of specimens.

$$\frac{\Delta}{\Delta_p} = \frac{P}{P_p}\left[1 + \alpha\left|\frac{P}{P_p}\right|^{r-1}\right]$$

Fig. 22   Ramberg-Osgood function.

respectively, while α and r are positive real numbers. This relationship is presented graphically in Fig. 22.

Equation (1) is the equation of the so-called "skeleton" or "backbone" curve[19,26]. Iwan[27] has attributed to Massing [Masing[28]] the suggestion that the hysteresis curve is identical in shape to the skeleton curve, but enlarged by a factor of two. Following Masing's hypothesis, then, the related hysteresis curve can be generated by Equation (2):

$$\frac{\Delta - \Delta_i}{2\Delta_p} = \frac{P - P_i}{2P_p}\left[1 + \alpha\left|\frac{P - P_i}{2P_p}\right|^{r-1}\right] \quad (2)$$

The point (Δ_i, P_i) is chosen as the point of last load reversal. These relationships are illustrated* in Fig. 23. The geometrical implications of Equations (1) and (2) have been explored in detail elsewhere[19,20].
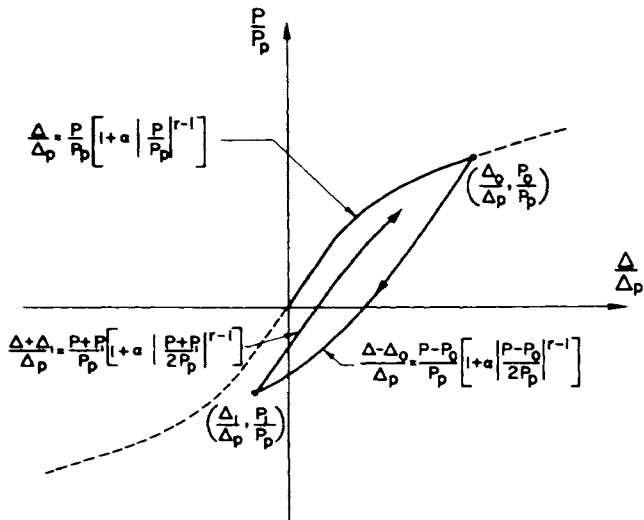
Equation (2) can be fitted by the

by Ramberg and Osgood[24] for the description of non-linear stress-strain curves, it has been adapted by Jennings[19], Kaldjian[25] and others to the present purpose and can be written thus:

$$\frac{\Delta}{\Delta_p} = \frac{P}{P_p}\left[1 + \alpha\left|\frac{P}{P_p}\right|^{r-1}\right] \quad (1)$$

where P and Δ are the load and deflection,

*After Kaldjian[25].

19

$$\frac{\Delta}{\Delta_p} = \frac{P}{P_p}\left[1+\alpha \left|\frac{P}{P_p}\right|^{r-1}\right]$$

$\left(\frac{\Delta_o}{\Delta_p}, \frac{P_o}{P_p}\right)$

$\frac{\Delta+\Delta_i}{\Delta_p} = \frac{P+P_i}{P_p}\left[1+\alpha \left|\frac{P+P_i}{2P_p}\right|^{r-1}\right]$

$\frac{\Delta-\Delta_o}{\Delta_p} = \frac{P-P_o}{P_p}\left[1+\alpha \left|\frac{P-P_o}{2P_p}\right|^{r-1}\right]$

$\left(\frac{\Delta_i}{\Delta_p}, \frac{P_i}{P_p}\right)$

Fig. 23   Masing's hypothesis.

method of least squares to experimentally obtained hysteresis curves. One approach is to fix the value of α and regard Δ_p, P_p, and r as adjustable parameters. Besides the fact that the elastic case is no longer included as a limiting case of Equation (1), however, it is often convenient to regard P_p and Δ_p as yield parameters, as shown in Fig. 20. If they are thus predetermined, adequate freedom of curve fitting requires that α be retained as an adjustable parameter. Furthermore, since the elastic slope is fixed by preselecting P_p and Δ_p, allowance must be made for any deviation of the unloading slope from the elastic slope (Fig. 23). Thus it is convenient to use for the hysteresis curve an equation of the form

$$\frac{\Delta-\Delta_i}{\Delta_p} = \frac{1}{\beta}\ \frac{P-P_i}{P_p}\left[1 + \alpha \left|\frac{P-P_i}{2P_p}\right|^{r-1}\right] \tag{3}$$

where β is such that $\beta(P_p/\Delta_p)$ is the slope of the unloading curve, and all other parameters and variables are as previously defined. An example of least squares fitting of Equation (2) to an experimental load-deflection hysteresis curve is shown in Fig. 24.

Because least squares curve fitting was prohibitively time-consuming for the large number of hysteresis diagrams acquired during the tests, and because certain corrections had to be applied to the data, an alternative

method was used in determining the parameters. The area enclosed by a hysteresis loop is found from Equation (3) to be

$$2W = \frac{r-1}{r+1}(P_2-P_1)\ \Delta \tag{4}$$

where the new variables are as defined in Fig. 25. Once the unloading slope and the enclosed area have been measured, α, β and r can be readily determined from Equations (4) and (3). This procedure was carried out for each half-cycle of every test for which load-deflection hysteresis diagrams were available.

The exponent r is a measure of the sharpness of curvature of the load-deflection curve; as r becomes very large, the curve approaches the elasto-plastic case. Excluding specimens of Type F3, because the hysteresis loops do not conform to the Ramberg-Osgood shape, the values of r obtained are summarized in Table IV. In general, r appears to be independent of the excursion number and, except at low amplitudes, of the plastic deflection.

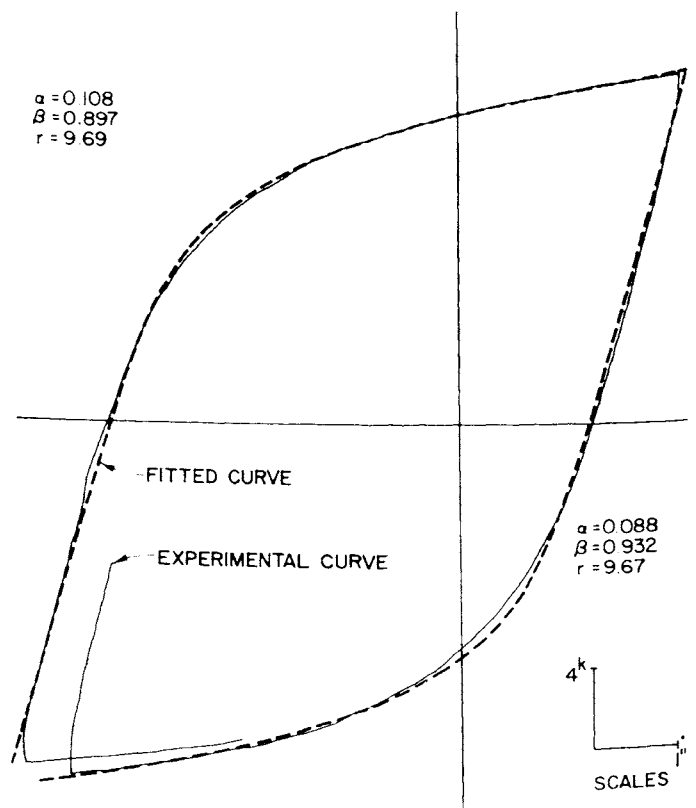The parameter α was found to be sensi-

$\alpha = 0.108$
$\beta = 0.897$
$r = 9.69$

FITTED CURVE

EXPERIMENTAL CURVE

$\alpha = 0.088$
$\beta = 0.932$
$r = 9.67$

4^k

SCALES

Fig. 24   Example of least-squares fit—specimen F1-C2.

20

TABLE IV: Ramberg-Osgood Exponent

Specimen Type	$r_{average}$
F1	9.05
F2	7.44
W1	8.42
W2	7.86

tive to small changes in the peak load level. The reason for this is apparent from Fig. 22. Conversely, however, the shape of the curve is affected but little by small changes in α. Although this parameter tended to show sudden large increase in later stages of several tests, it is felt that the earlier values are of greatest applicability in the range of loading likely to be encountered in a real structure. Hence only those values have been averaged in Table V.

TABLE V: Parameter α

Specimen Type	$\alpha_{average}$
F1	0.48
F2	0.48
W1	0.45
W2	0.68

Usually, α increased slowly with increasing load, until the occurrence, if any, of the sudden increase mentioned above.
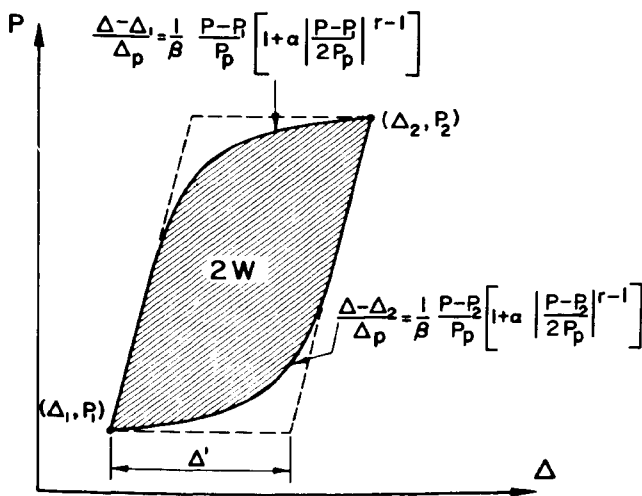
Fig. 25 Hysteresis area.

The slope factor β is a measure of the stiffness of a specimen. As such, it was found to be indicative of the onset and degree of buckling. In those cases where buckling was essentially absent, such as in specimen F2-C4, β remained close to unity, decreasing somewhat in only the last few cycles before failure. Where pronounced buckling occurred early in the history of the specimen, and continued to increase during cycling, β was found to decrease steadily, as for specimens F1-C2, F1-C6, F2B-C8 and others.

For practical use, recommended values of the Ramberg-Osgood parameters are $\alpha = 0.5$, $\beta = 1$ and $r = 8$. The use of the absolute value function in Equations (1), (2) and (3) can be avoided by choosing an odd integer for the value of r; in this case $r = 9$ is recommended.

Ductility Factor

A widely used measure of the cyclic post-yield behavior of a structure is the so-called ductility factor, denoted by μ. The ratio of total deformation to elastic deformation at yield, it has been variously defined as that ratio for strains[25], rotations[29] and displacements[30]. The value of the ductility factor thus varies widely, depending upon the definition used. That for strain presumably depends almost exclusively on the material, while that for rotation adds the effects of the shape and size of cross section. When applied to displacements, the entire configuration of structure and loading is incorporated. Another source of confusion arises over whether the ductility factor is measured consistently from the initial configuration of the system, or from the immediately preceding no-load configuration. Thus, in any discussion of the ductility factor, it is important to bear in mind the definition used. Moreover, it becomes difficult to generalize on the adequacy, or lack thereof, of the ductility so measured.

Plasticity Ratio

The above definition of the ductility factor is perhaps unfortunate, in that it includes the recoverable deformation as well as the permanent, or plastic, deformation. Furthermore, it is best suited to steady-state

21

response, as it is otherwise inconvenient to keep track of the residual displacement at no load. It is thus awkward to use as a cumulative damage indicator. A more logical measure would seem to be the ratio of residual plastic deformation to elastic deformation at yield. For convenience, this ratio will be referred to as the "deflection plasticity ratio", or simply the "plasticity ratio", denoted by π_d. By restricting the definition in this way, the ambiguities associated with the ductility factor, as outlined above, can be completely avoided. The ductility factor μ and plasticity ratio π_d, as used in this report, are defined in Fig. 26.
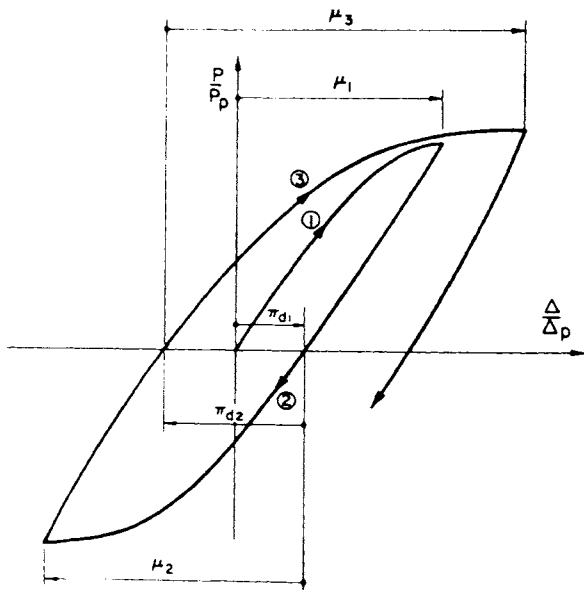
Fig. 26 Definition of ductility factor μ and plasticity ratio π_d

The magnitude of the plasticity ratio or ductility factor which could be achieved was found to be simply a matter of how much deflection was applied to the beam. The maximum values applied to the specimen are given in Table VI. It is emphasized that these are maximum values applied. In no case should it be construed that an entire test was conducted with the tabulated value; nor should it be construed that larger values could not be attained for any specimen.

Cyclic Energy Dissipation

The dynamic response of a structure is markedly influenced by the amount of energy absorbed and dissipated during motion. Since response is usually described in terms of displacement, it is of interest to know how the cyclic energy dissipation is related to displacement. Jennings[20] has shown this relationship in terms of total displacement for steady-state response, and based on the Ramberg-Osgood hysteresis shape. Once again, however, the random nature of earthquake response makes it inconvenient to employ the total displacement in this manner. Hence the permanent deformation, as incorporated into the previously defined deflection plasticity ratio π_d, will be used.

It is convenient to define a dimensionless energy ratio $e = W/(\frac{1}{2}P_p\Delta_p)$ based on the energy dissipated during a single excursion*. The relationship between e and π_d for each excursion for every specimen, including those of Type F3, for which load-deflection data were available, is shown in Fig. 27.

It may be noted that for low values of π_d, the points are well clustered near the least-squares fitted line. Points enclosed by triangles include data for the A-441 specimens. It is not surprising that they also fall near the line, since the hysteresis area is geometrically related to the plastic deflection in the same way regardless of the strength of the steel, provided that the shapes of the diagrams are similar. It is interesting, however, that the data for the bolted connections are also included, in that their hysteresis curves are not well described by the Ramberg-Osgood function.

Although the matter is argumentative, it has been suggested [29] that a ductility ratio of the order of 4 might be experienced in a structure. This would correspond to a plasticity ratio of about 3, so that the lowermost portion of the diagram of Fig. 27 is by far the most significant. Thus the line shown is proposed as a reasonable estimate for relating the energy absorption to the plastic displacement for at least the two types of steel tested. The equation of this line is

$$e = 1.77\,\pi_d \qquad (5)$$

---

*Note that for steady-state response, this is precisely one-half of the energy ratio defined by Jennings.
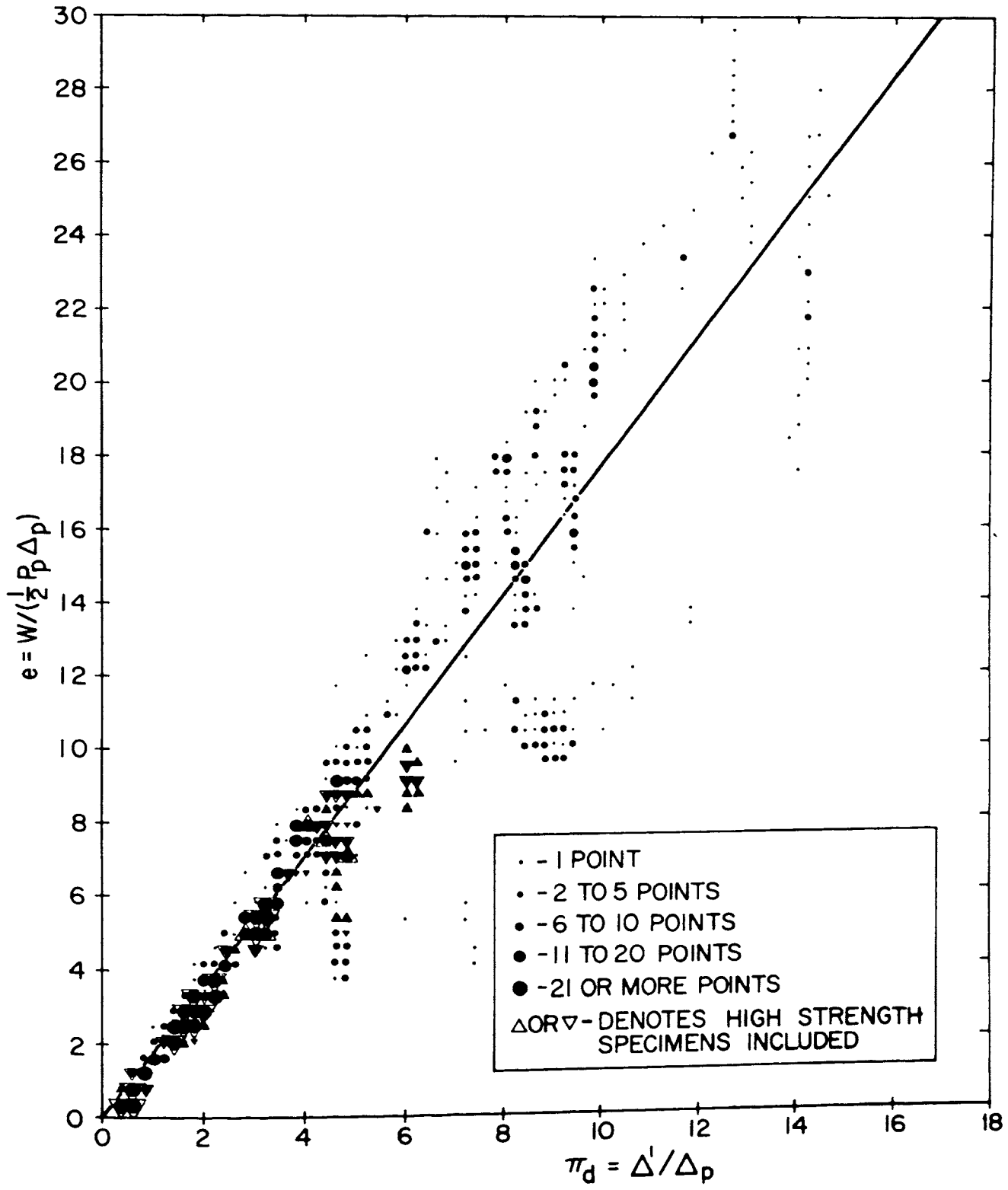
22

Fig. 27   Energy ratio versus plasticity ratio.

Cumulative Engergy Dissipation

Energy dissipation has been suggested as a criterion of cumulative damage[14]. One way to describe the history of a specimen, then, is to plot the cumulative energy absorption throughout that history. Figs. 28 and 29 show these data for all specimens. The slope of each curve indicates the rate of energy absorption, while its terminus indicates the point at which failure occurred. Both the total energy and the number of excursions to failure can be read from this point.

It will be noticed that the Type F1 specimens show consistently high energy-absorbing capabilities, even at high rates of absorption. Furthermore, the specimens of both types of steel performed well.

On the whole, none of the other specimen types performed as well as F1, in terms of actual energy absorption capability. Again, however, in the case of Type F2, no superiority of one steel over the other could be discerned. A particularly interesting aspect of the general performance is illuminated by a consideration of the Type F3 specimens. Specimen F3-C5 had the thickest plates,

F3A-C7 thinner, and F3B-C7, thinner yet. Failure (that is, opening of a crack) occurred in F3-C5 at the net section of the beam, and in F3B-C7, at the net section of the plates. In specimen F3A-C7, however, with the plates of intermediate thickness, failure occurred simultaneously at the net section of both beam and plates. This specimen was able to sustain a considerably larger energy input than either of the other two, leading to the conclusion that the greater the volume of material over which the damage can be spread, the longer the life of the specimen. The better performance of Type F1 specimens can therefore presumably be attributed to the severe flange buckling, while damage was necessarily more localized in the plated connections. This would also account, at least in part, for the somewhat less satisfactory performance of the W-type connections, in that the stress concentrations resulting from their configurations once again localized the damage. It is concluded that, in general, a relatively stiffer connection will suffer in comparison with another more flexible one of the same strength.

TABLE VI: Maximum Applied Ductility Factors and Plasticity Ratios

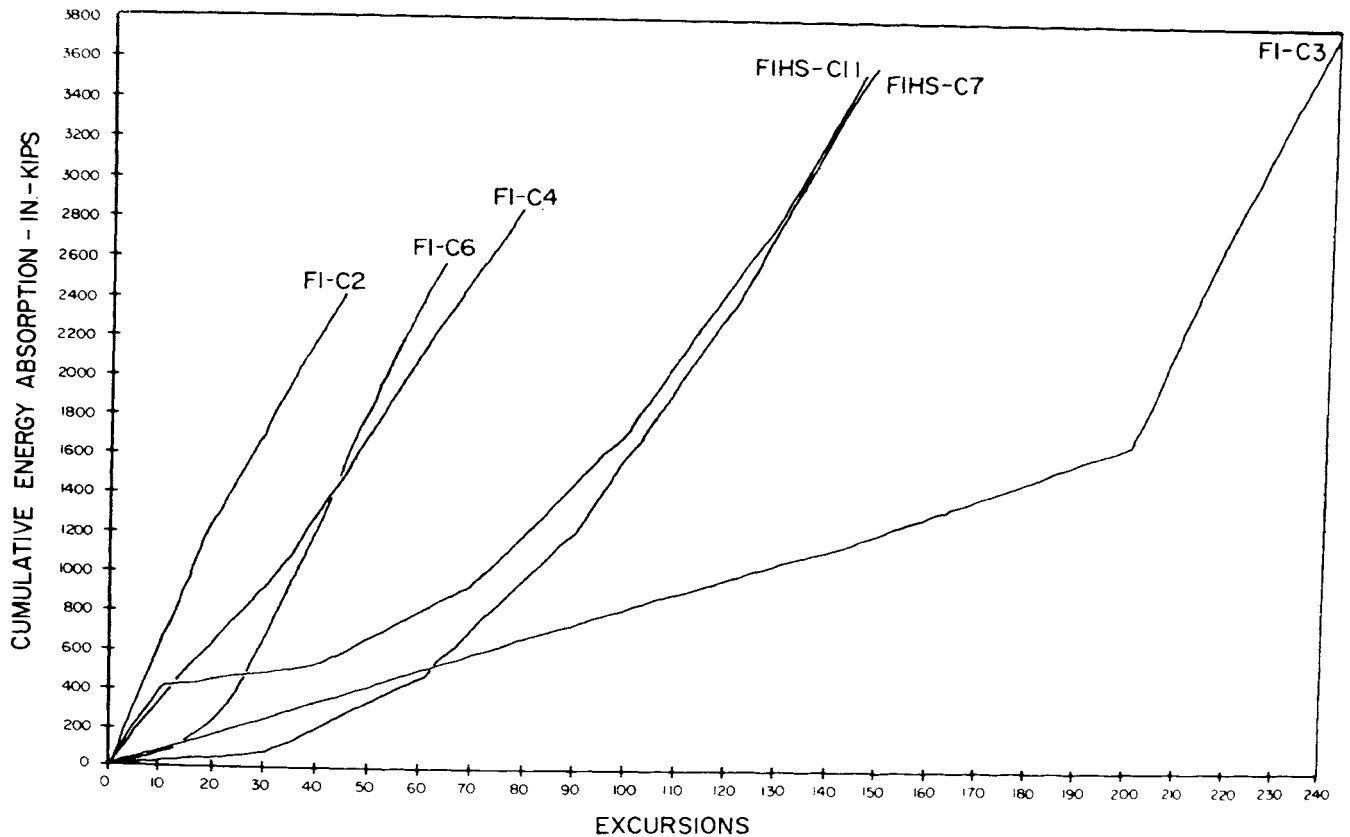| Specimen	$(^\pi d)$ max	μ_{max}	Specimen	$(^\pi d)$ max	μ_{max}
F1-C1	12.2	13.9	F3A-C7	12.7	14.8
F1-C2	12.3	13.8	F3B-C7	8.3	9.8
F1-C3	8.3	9.7	W1-C1	2.2	3.5
F1-C4	9.5	11.2	W1-C7	3.4	5.0
F1-C6	14.5	16.1	W1-C9	4.8	6.2
F2-C1	9.8	11.3	W2A-C7	4.6	5.8
F2-C4	5.7	7.2	W2B-C10	3.6	4.8
F2A-C7	5.0	6.3	F1HS-C7	5.8	7.4
F2B-C8	7.3	8.5	F1HS-C11	6.0	7.2
F3-C1	13.3	15.0	F2HS-C7	3.0	4.2
F3-C5	11.8	13.4	F2HS-C9	4.8	6.2

Fig. 28 Cumulative energy absorption.

Total Energy Dissipation

The total energy dissipated by each specimen can be read from Figs. 28 and 29, as previously explained. It is possible, however, to present the failure points in terms of the accumulated energy ratio Σe and the accumulated plasticity ratio $\Sigma \pi_d$, where each summation is carried out over the total number of excursions for each test. These data are shown in Figure 30.

The strength and stiffness of each specimen have now been incorporated into the diagram. The greater the distance of a given point from the origin, the greater, in some sense, is the energy absorption capability of a specimen. On this basis, with the exception of specimen type F3A-C7, specimen type F1 appears again to perform best, although the A-441 specimens were not able to sustain as high total energy ratios as did those of A-36 steel. Some of the reasons for the apparently exceptional performance of specimen F3A-C7 have already been discussed; it is noted that its strength was based upon its net section and was thus quite low, raising the energy ratios.

Figure 30 indicates that the total energy ratio at any time in the history of a specimen is simply related to the toal plasticity ratio as accumulated to that time. Thus, if the history of plastic deformation of a connection is known, it is possible to obtain some idea of its expected life, if it is at all similar to any of the specimen configurations tested. Obviously, this procedure is extremely subject to the interpretation of the designer or analyst and, as stated at the outset. is qualitative only.

Comparison of Steels

Having demonstrated experimentally some of the relative performance characteristics of the two steels tested. it is of interest now to examine the analytical implications of the choice of steel. This will be done by comparing designs based on the requirements of (1) equal strength. and (2) equal stiffness. To make a simple comparison, it is necessary to hold certain parameters fixed while varying the yield strength:

1. The type of structure and loading is

25
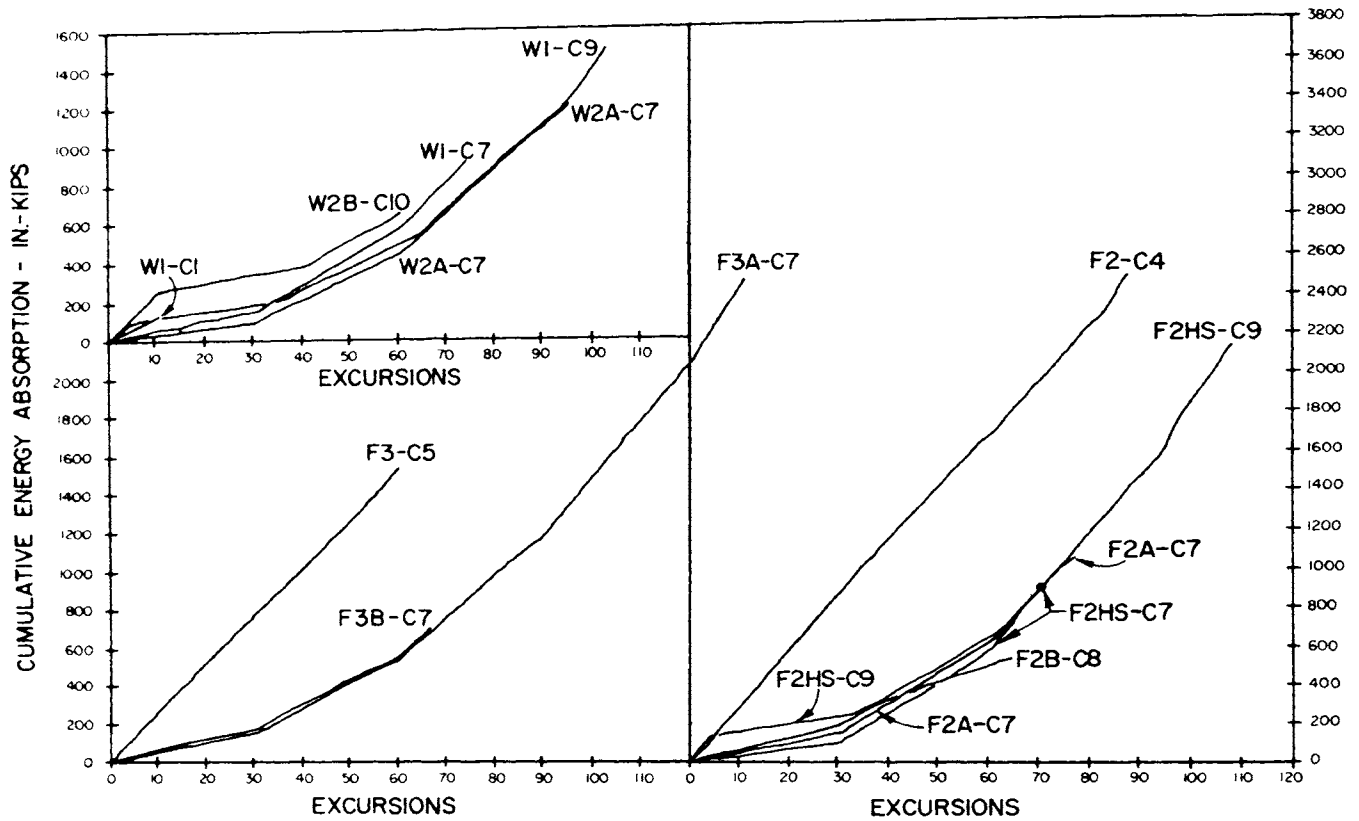
Fig. 29 Cumulative energy absorption.

assumed to be the same, viz., a cantilever beam of fixed length and carrying a concentrated load at the free end.

2. The cross section is assumed to be of the same depth and to have the same shape factor.

As is well known, the elastic modulus is practically constant, regardless of the strength of the steel.

With these assumptions, two structures of equal strength are related as follows: both can support the same ultimate plastic load, but the elastic deflections corresponding to this load level differ by the ratio of the yield strengths. Symbolically:

$$P_{p2} = P_{p1} \quad and \quad \Delta_{p2} = \frac{\sigma_{y2}}{\sigma_{y1}} \Delta_{p1}$$

Similarly, two structures of equal stiffness can be related: the respective ultimate plastic loads differ by the ratio of the yield strengths, as do also the corresponding elastic deflections. Hence,

$$P_{p2} = \frac{\sigma_{y2}}{\sigma_{y1}} P_{p1} \quad and \quad \Delta_{p2} = \frac{\sigma_{y2}}{\sigma_{y1}} \Delta_{p1}$$

Note that under the assumptions, equal stiffness design is achieved by using members of identical cross section. Using typical values of r and α, and taking $\beta = 1$, the skeleton curves for the three cases are shown in Fig. 31.

From these skeleton curves, it is now possible to generate the corresponding hysteresis loops. Four comparisons are made in Fig. 32: (a) equal strength—equal load, (b) equal strength—equal deflection, (c) equal stiffness—equal load, and (d) equal stiffness—equal deflection. In each case, the shaded area represents the performance of the A-36 steel structure. Although the designer must interpret these comparisons himself in light of his particular structure, some general remarks can be made. First, the effects of equal strength design are not nearly so dramatic as are those of equal stiffness design. It appears that the performance of equal strength structures would be similar, although presumably

26
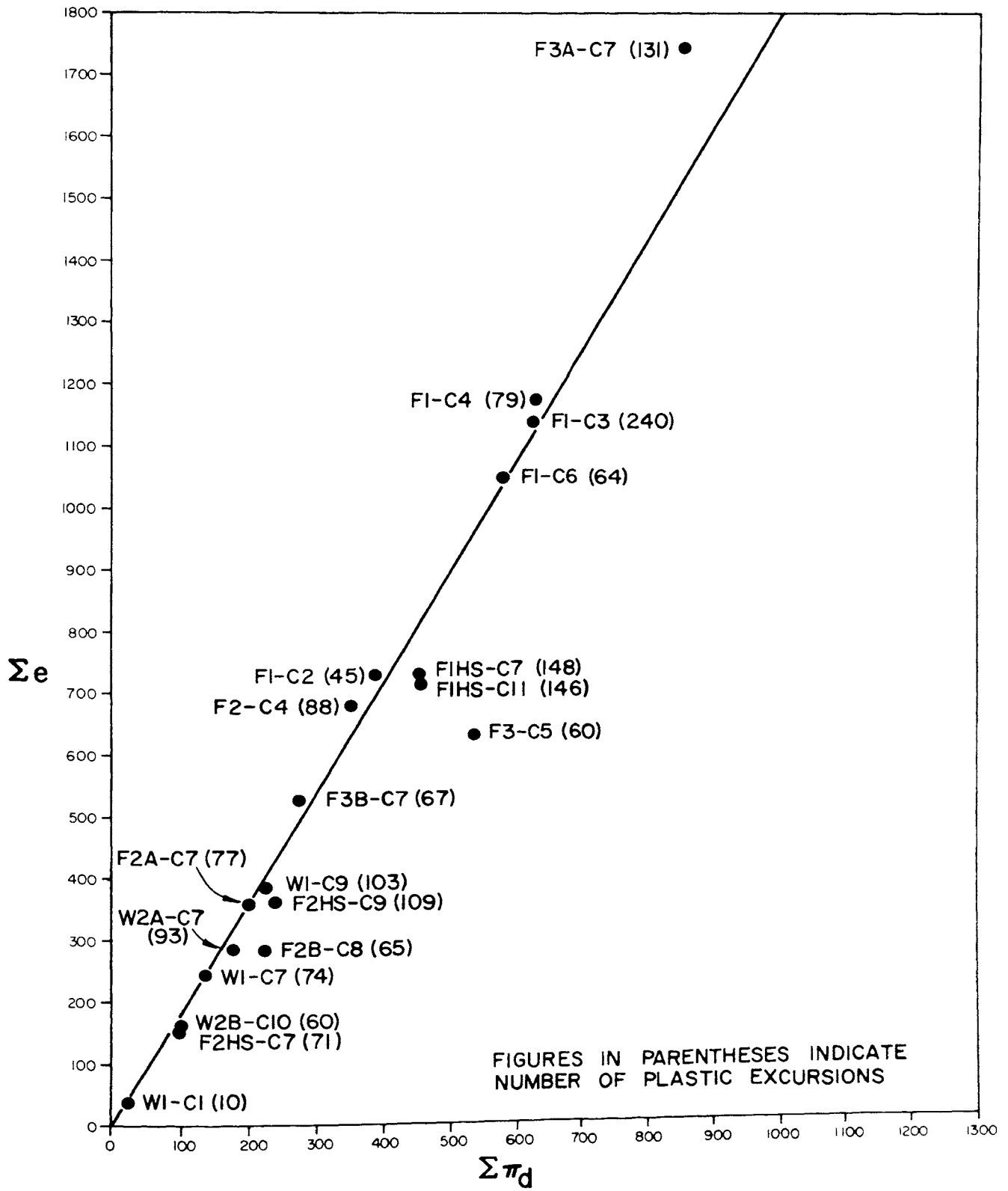
Fig. 30   Accumulated energy ratio versus accumulated plasticity ratio.
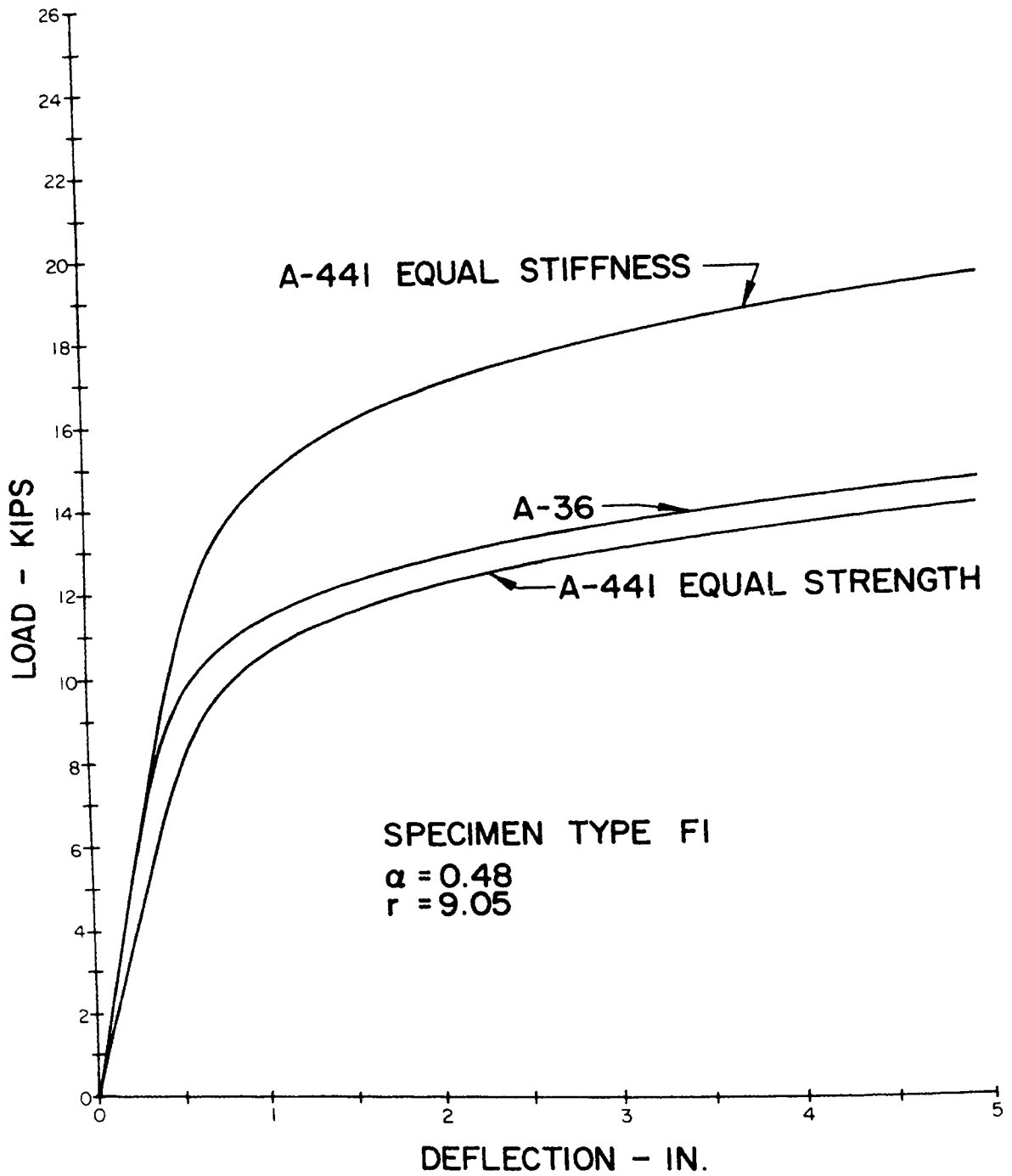
Fig. 31   Comparison of A-36 and A-441 steels.
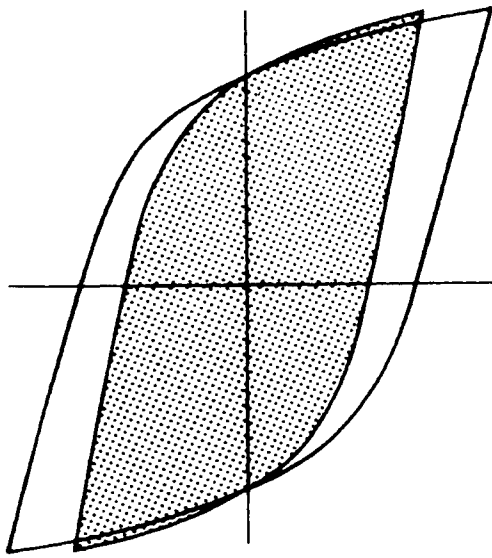
(a)
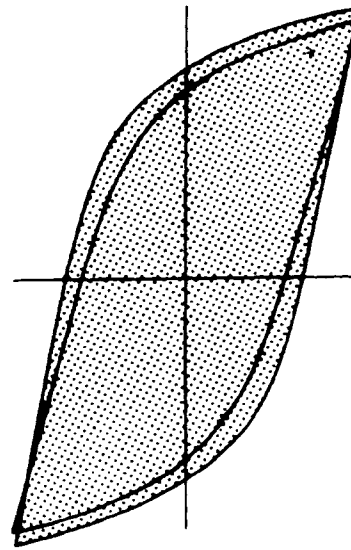
(b)

EQUAL STRENGTH DESIGN
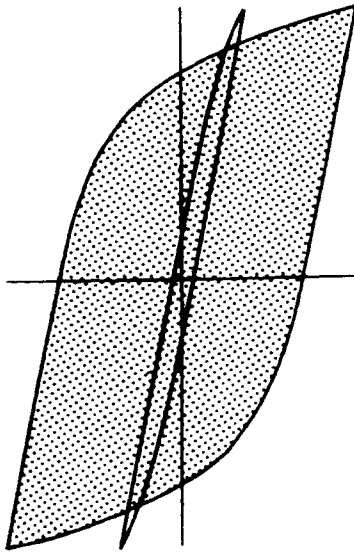
(c)

(d)
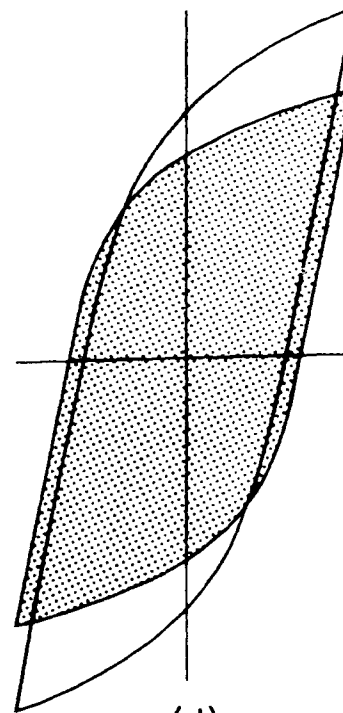
EQUAL STIFFNESS DESIGN

Fig. 32   Comparison of equal strength and equal stiffness
designs. Shaded loops are for A-36 steel; others are
for A-441 steel.

29

somewhat larger deformations could be expected in the A-441 structure. In the case of structures of equal stiffness, however, considerably larger loads might be required to mobilize the intrinsic energy-absorbing capabilities. On the other hand, if the load responses are of the same order of magnitude, it is apparent that the capacity of the structure would be used up very slowly. It must be reiterated, then, that there is no simple answer to the question of which steel is preferable; it depends upon the specific application, and must be left to the judgment of the designer.

CONCLUSIONS

Based on the results of this investigation, a number of conclusions can be reached. Some of these are of immediate significance to the designer; others may be of importance for future research.

1. The load-deflection hysteresis loops for a steel cantilever beam and connection are highly reproducible during repetitive load application. This implies that such an assemblage is very reliable, and can be counted upon to absorb a definite amount of energy in each cycle for a prescribed displacement.

2. Using total energy absorption as the sole criterion, the performance of specimen type F1 in general excelled that of any other type. No clear superiority was apparent among the other types of connection. All sustained loads in excess of their design limit loads until the onset of cracking.

3. The ability to withstand severe repeated and reversed loading seems to be assured for properly designed and fabricated steel connections; their intrinsic energy absorption capacity is large. Moreover, the number of repeated and reversed loadings which can be safely sustained appears to be in excess of that which may be anticipated in actual service, although this requires justification by means of dynamic analysis of buildings subjected to seismic action.

4. The performance of specimens of A-441 steel was comparable to that of specimens of A-36 steel. In the specimens tested, higher loads were developed because of geometric similarity. Energy absorption capability of A-441 was as good as or better than that for A-36 steel. The choice of steel depends upon the particular application.

5. The importance of careful inspection during fabrication was brought out by the premature failure of two improperly welded connections.

6. It has been demonstrated that local flange buckling did not precipitate an immediate loss of load-carrying capacity. Indeed, the ability to buckle and thus distribute damage may be of significance in prolonging the life of a member. Such distribution of damage, or lack thereof, has been related qualitatively to the respective longevities of the specimens tested.

7. The energy absorption capacity, as measured by the size of the hysteresis loops, increases with increasing tip-deflection. A simple linear dependence of the dissipated energy per cycle upon the residual deflection has been suggested. The plasticity ratio has been defined and proposed as a more useful measure of post-yield performance than the ductility factor.

8. The mathematical representation of a hysteresis curve using the Ramberg-Osgood relationship has been found to be highly satisfactory, in the absence of slip, justifying its use in analysis of structures subjected to inelastic load reversal.

9. It does not appear possible on the basis of these tests to formulate a rational approach to the prediction of total energy absorption capacity. Only a qualitative assessment may be made by means of direct comparison with actual test results. Finally, it must be emphasized that this report is based entirely on a single beam size, 8 WF 20. Extrapolation to members with other cross sections must be done with caution.

REFERENCES

1. *Commentary on Plastic Design in Steel,* American Society of Civil Engineers, Manual of Engineering Practice No. 41, New York, 1961.
2. Beedle, L. S., *Plastic Design of Steel Frames,* John Wiley and Sons, New York, 1958.
3. Neal, B. G., *The Plastic Methods of Structural Analysis,* John Wiley and Sons, New York, 1956.
4. Hodge, P. G., Jr., *Plastic Analysis of Structures,* McGraw-Hill Book Co., New York, 1959.
5. Timoshenko, S., *Strength of Materials,* Part II, 3rd edition, Van Nostrand, Princeton, N. J., March 1956.
6. Popov, E. P., *Introduction to Mechanics of Solids,* Prentice-Hall, Englewood Cliffs, N. J., 1968.
7. Bresler, B., T. Y. Lin and J. B. Scalzi, *Design of Steel Structures,* 2nd edition, John Wiley and Sons, New York, 1968.
8. Symonds, P. S. and B. G. Neal, "Recent Progess in the Plastic Methods of Structural Analysis," *Journal of the Franklin Institute,* 252, 1951, pp. 383-407 and 469-492.
9. Bertero, V. V. and E. P. Popov, "Effect of Large Alternating Strains on Steel Beams," *Journal of the Structural Division,* ASCE, Vol. 91, No. ST1, February, 1965, pp. 1-12.
10. Popov, E. P., "Behavior of Steel Beam-to-Column Connections under Repeated and Reversed Loading," *Summer Conference on Plastic Design of Multi-Story Frames,* Fritz Engineering Laboratory, Lehigh University, 1965, pp. 241-260.
11. Popov, E. P. and H. A. Franklin, "Steel Beam-to-Column Connections Subjected to Cyclically Reversed Loading," *Proceedings,* Structural Engineers Association of California, October, 1965.
12. Popov, E. · P., "Low-Cycle Fatigue of Steel Beam-to-Column Connections," *International Symposium on the Effect of Repeated Loading on Materials and Structures,* RILEM-Instituto de Ingeneria, Vol. VI, Mexico City, September, 1966.
13. Popov, E. P. and R. B. Pinkney, "Alternating Inelastic Strains in Steel Connections," unpublished paper presented to the National Meeting of the American Society of Civil Engineers, Seattle, Washington, May, 1967.
14. Morrow, Jo Dean, "Cyclic Plastic Strain Energy and Fatigue of Metals," *Internal Friction, Damping and Cyclic Plasticity,* ASTM, STP-378, 1965, p. 77.
15. Benham, P. P. and H. Ford, "Low Endurance Fatigue of a Mild Steel and an Aluminum Alloy," *Journal of Mech. Eng. Science,* Vol. 3, No. 2, June, 1961, pp. 119-132.
16. Ruzicka, J. E., editor, *Structural Damping,* papers at colloquium, ASME, Appl. Mech. Div., New York, December, 1959.
17. Berg, G. V., "A Study of the Earthquake Response of Inelastic Systems," *Proceedings,* Structural Engineers Association of California, October, 1965.
18. Goel, S. C., "The Response of Steel Frame Structures to Earthquake Forces, Part II, Multiple-Degree-of-Freedom Systems," *Report No. 06869-2-F,* Department of Civil Engineering, The University of Michigan, December, 1967. Published as American Iron and Steel Institute Bulletin 12, 1968.
19. Jennings, Paul C., "Periodic Response of a General Yielding Structure," *Journal of the Engineering Mechanics Division,* ASCE, Vol. 90, No. EM2, Proc. Paper 3871, April, 1964, pp. 131-166.
20. Jennings, Paul C., "Earthquake Response of a Yielding Structure," *Journal of the Engineering Mechanics Division,* ASCE, Vol. 91, No. EM4, Proc. Paper 4435, August, 1965, pp. 41-68.
21. Hanson, R. D., "Comparison of Static and Dynamic Hysteresis Curves," *Journal of the Engineering Mechanics Division,* ASCE, Vol. 92, No. EM5, Proc. Paper 4949, October, 1966, pp. 87-113.
22. Popov, E. P. and R. B. Pinkney, "Behavior of Steel Building Connections Subjected to Repeated Inelastic Strain Reversal–Experimental Data," *Report No. SESM 67-31,* Structural Engineering Laboratory, University of California. (Bulletin 14, American Iron and Steel Institute).
23. Douty, R. T., and W. McGuire, "High Strength Bolted Moment Connections," *Journal of the Structural Division,* ASCE, Vol. 91, No. ST2, Proc. Paper 4298, April, 1965, pp. 101-128.
24. Ramberg, W. and W. R. Osgood, "Description of Stress-Strain Curves by Three Parameters," *Technical Note 902,* NACA, July, 1943.
25. Kaldjian, M. J., "Moment-Curvature of Beams as Ramberg-Osgood Functions," *Journal of the Structural Division,* ASCE, Vol. 93, No. ST5, Proc. Paper 5488, October, 1967, pp. 53-65.
26. Medearis, K. and D. H. Young, "Energy Absorption of Structures Under Cyclic Loading," *Journal of the Structural Divison,* ASCE, Vol. 90, No.

ST1, Proc. Paper 3791, February, 1964, pp. 61-91.

27. Iwan, W. D., "On a Class of Models for the Yielding Behavior of Continuous and Composite Systems," *Journal of Applied Mechanics,* ASME, Vol. 34, No. 3, September, 1967, pp. 612-617.

28. Masing, G., "Eigenspannungen und Verfestigung beim Messing," *Proceedings of the Second International Congress for Applied Mechanics,* Zurich, September, 1926.

29. Hanson, N. W. and H. W. Conner, "Seismic Resistance of Reinforced Concrete Beam-Column Joints," *Journal of the Structural Division,* ASCE, Vol. 93, No. ST5, Proc. Paper 5537, October, 1967, pp. 533-560.

30. Blume, J. A., N. M. Newmark and L. H. Corning, *Design of Multi-Story Reinforced Concrete Buildings for Earthquake Motions,* Portland Cement Association, Skokie, Ill., 1961.

REVIEW AND SUMMARY OF JAPANESE RESEARCH
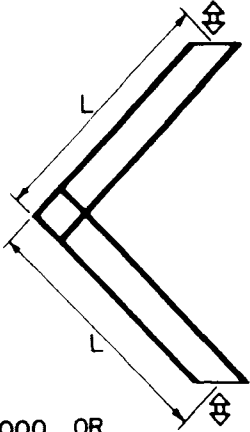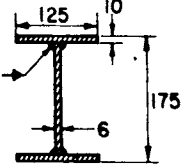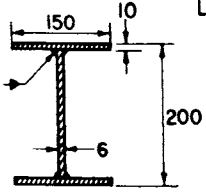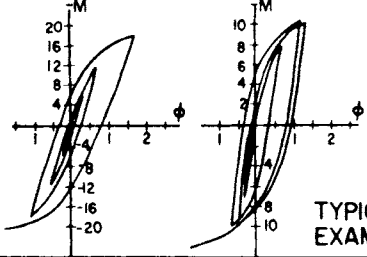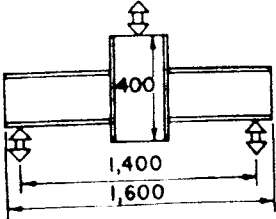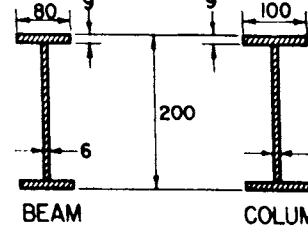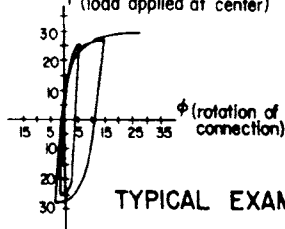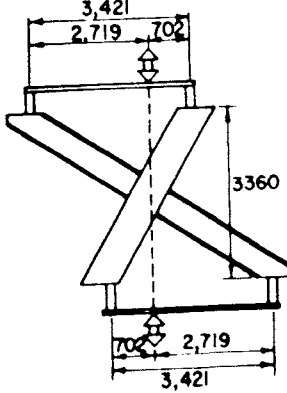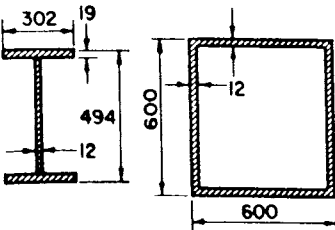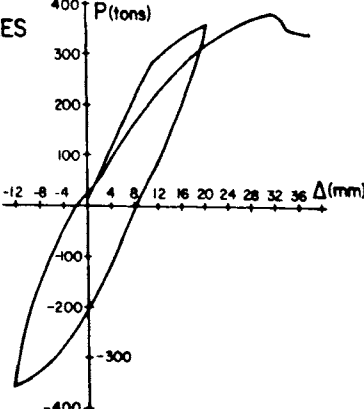
As stated in the Introduction, much research has been done in Japan on the behavior of steel beam-to-column connections and assemblages. This work is reported in a number of technical publications which may not be readily accessible to American readers. As an aid to overcoming this difficulty, a considerable body of Japanese literature on the subject has been reviewed, and selections of what appeared to be the most important original work have been made and summarized in the following few pages. The information is presented graphically so that some idea of the principal investigations can be quickly obtained. The reader who is interested in further details will find references to the source material at the end of the summary. Note that all dimensions are given in metric units.
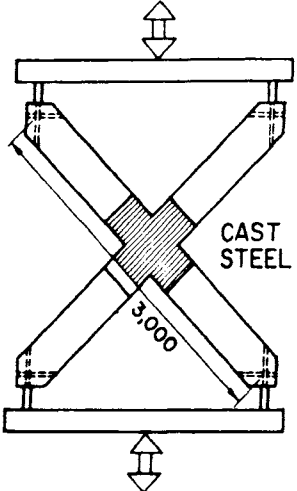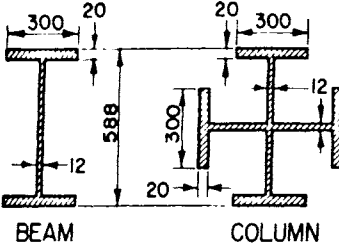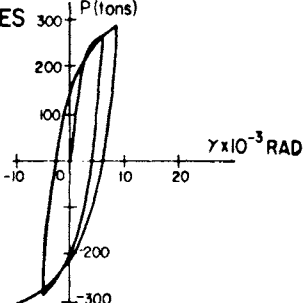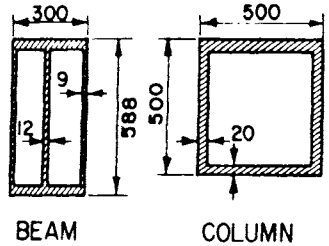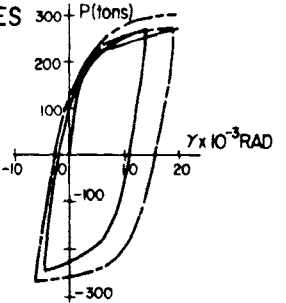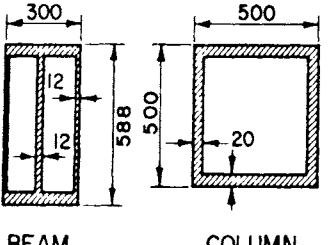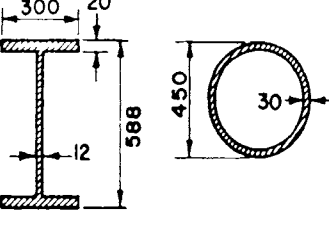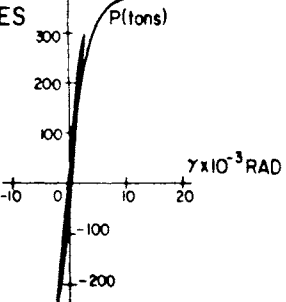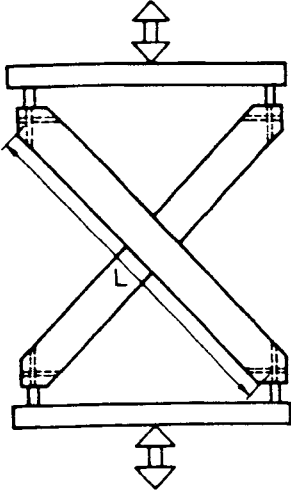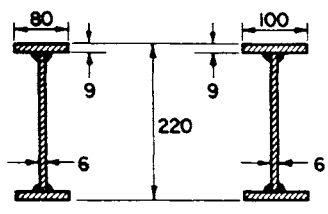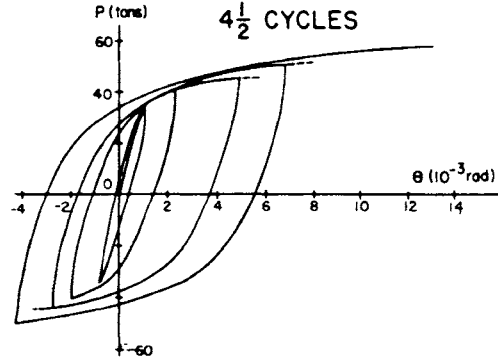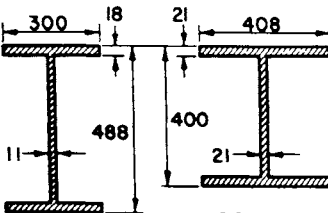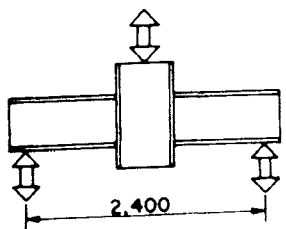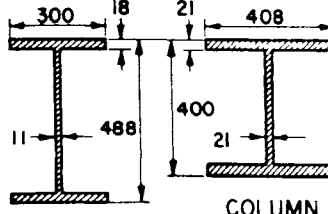
Professor Masahide Tomii of the University of Kyushu, during his residence in 1966 as a Research Associate at the University of California, Berkeley, was principally responsible for making the selections for the summary. Dr. Makoto Watabe of the International Institute of Seismology and Earthquake Engineering, currently Research Associate at the University of California, assisted with the final organization of the summary.

REFERENCES TO THE APPENDIX

A1. Igarashi, S., J. Sumida and M. Tomoda, "Report on the Elastic and Plastic Behavior of Steel Connections Subjected to Cyclic Load," *Transactions of the Architectural Institute of Japan,* Vol. 69, October, 1961.

A2. Igarashi, S., J. Sumida and J. Sakamoto, "Experimental Study of the Hysteresis Characteristics of Steel Connections with Relation to the Damping Properties of a Structure," *Transactions of the Architectural Institute of Japan,* Vol. 75, August, 1962.

A3. Naka, T., B. Kato, T. Sasaki and M. Nakao, "Report on the Hysteresis Characteristics and Strength of Steel Beam-to-Column Connections Subjected to Cyclic Load," *Architectural Institute of Japan,* Spring Seminar in Kanto, May, 1963.

A4. Naka, T., B. Kato, M. Watabe, A. Tanaka and T. Sasaki, "Research on the Behavior of Steel Beam-to-Column Connections Subjected to Lateral Force—Report No. 1," *Trans. of the Arch. Inst. of Japan,* Vol. 101, August, 1964.

A5. Naka, T., B. Kato, M. Watabe, A. Tanaka and T. Sasaki, "Research on the Behavior of Steel Beam-to-Column Connections Subjected to Lateral Force—Report No. 2," *Trans. of the Arch. Inst. of Japan,* Vol. 102, September, 1964.

A6. Naka, T., B. Kato, M. Watabe, A. Tanaka and T. Sasaki, "Research on the Behavior of Steel Beam-to-Column Connections Subjected to Lateral Force—Report No. 3," *Trans. of the Arch. Inst. of Japan,* Vol. 103, October, 1964.

A7. Naka, T., B. Kato, M. Watabe and A. Tanaka, "Experimental Study on the Behavior of Steel Beam-to-Column Connections with High Tensile Strength Bolts," *International Association of Bridge and Structural Engineering,* Seminar of Japanese Branch, November, 1965.

TYPE OF EXPERIMENT	SIZE OF MEMBERS - mm	STEEL PROPERTIES	NUMBER OF SPECIMENS	REMARKS	REFERENCE NUMBER
L=1,000 OR 1,200 mm	125, 10, 175, 6 — L=1,000 mm	SS 41 P FOR 6mm PLATE: F_y=28.5 kg/mm^2 F_u=43.1 kg/mm^2 FOR 10mm PLATE: F_y=30.3 kg/mm^2 F_u=46.0 kg/mm^2	21	TYPICAL EXAMPLES	A1
	150, 10, 200, 6 — L=1,200 mm		12	TYPICAL EXAMPLE	A2
400, 1,400, 1,600	80, 9, 9, 100, 200, 6, 6 BEAM COLUMN	FOR 6mm PLATE: F_y=28.2 kg/mm^2 F_u=40.6 kg/mm^2 FOR 9mm PLATE: F_y=26.0 kg/mm^2 F_u=46.2 kg/mm^2	5	3½ CYCLES TYPICAL EXAMPLE	A3
3,421, 2,719, 702, 3360, 702, 2,719, 3,421	302, 19, 600, 494, 12, 12, 600, 600	FOR 19mm PLATE: F_y=37.1 kg/mm^2 F_u=55.7 kg/mm^2 FOR 12mm PLATE: F_y=410 kg/mm^2 F_u=60.6 kg/mm^2	1	1½ CYCLES	A4

TYPE OF EXPERIMENT	SIZE OF MEMBERS - mm	STEEL PROPERTIES	NUMBER OF SPECIMENS	REMARKS	REFERENCE NUMBER
	 BEAM COLUMN	SS 41 $F_y = 24.1$ kg/mm^2 $F_u = 44.1$ kg/mm^2	2	 2 CYCLES	A5
	 BEAM COLUMN	BEAM SS 41: $F_y = 24.1$ kg/mm^2 $F = 44.1$ kg/mm^2 COVER PLATES SM 50 F_y and F_u not given	1	 1$\frac{1}{2}$ CYCLES	A5
	 BEAM COLUMN	but probably $F_y = 36.0$ kg/mm^2 $F_u = 53.4$ kg/mm^2 COLUMNS CAST STEEL $F_y = \cdot33.0$ kg/mm^2 $F_u = 51.5$ kg/mm^2	1	1$\frac{1}{2}$ CYCLES	A5
	 BEAM COLUMN	BEAM SS 41: $F_y = 24.1$ kg/mm^2 $F_u = 44.1$ kg/mm^2 COLUMN CAST STEEL $F_y = 41.4$ kg/mm^2 $F_u = 60.2$ kg/mm^2	1	 1$\frac{1}{2}$ CYCLES	A5

TYPE OF EXPERIMENT	SIZE OF MEMBERS - mm	STEEL PROPERTIES	NUMBER OF SPECIMENS	REMARKS	REFERENCE NUMBER
	L = 798 mm 80, 100, 9, 9, 220, 6, 6 BEAM COLUMN	FOR 6mm PLATE: Fy = 28.2 kg/mm^2 Fu = 40.6 kg/mm^2 FOR 9mm PLATE: Fy = 26.0 kg/mm^2 Fu = 46.2 kg/mm^2	5	 TYPICAL EXAMPLE	A 6
	L = 3,000 mm 300, 18, 21, 408, 488, 400, 11, 21 BEAM COLUMN	BEAM: Fy = 39.5 kg/mm^2 Fu = 53.0 kg/mm^2 COLUMN: Fy = 35.3 kg/mm^2 Fu = 53.3 kg/mm^2	4	2½ TO 3½ CYCLES	A 7
  2,400	300, 18, 21, 408, 488, 400, 11, 21 BEAM COLUMN	BEAM: Fy = 39.5 kg/mm^2 Fu = 53.0 kg/mm^2 COLUMN: Fy = 35.3 kg/mm^2 Fu = 53.3 kg/mm^2	4	1½ TO 2½ CYCLES	A 7

BULLETINS

Steel Research for Construction